Oncogene
https://doi.org/10.1038/s41388-019-0988-y

ARTICLE

A gain-of-functional screen identifies the Hippo pathway as a central mediator of receptor tyrosine kinases during tumorigenesis

Taha Azad[1] · Kazem Nouri[1] · Helena J. Janse van Rensburg[1] · Sarah M. Maritan[1] · Liqing Wu[1] · Yawei Hao[1] · Tess Montminy[1] · Jihang Yu[1] · Prem Khanal[1] · Lois M. Mulligan[1] · Xiaolong Yang[1]

Received: 2 January 2019 / Revised: 3 July 2019 / Accepted: 5 July 2019

Abstract

The Hippo pathway has emerged as a key signaling pathway that regulates various biological functions. Dysregulation of the Hippo pathway has been implicated in a broad range of human cancer types. While a number of stimuli affecting the Hippo pathway have been reported, its upstream kinase and extracellular regulators remain largely unknown. Here we performed the first comprehensive gain-of-functional screen for receptor tyrosine kinases (RTKs) regulating the Hippo pathway using an RTK overexpression library and a Hippo signaling activity biosensor. Surprisingly, we found that the majority of RTKs could regulate the Hippo signaling activity. We further characterized several of these novel relationships [TAM family members (TYRO3, AXL, METRK), RET, and FGFR family members (FGFR1 and FGFR2)] and found that the Hippo effectors YAP/TAZ are central mediators of the tumorigenic phenotypes (e.g., increased cell proliferation, transformation, increased cell motility, and angiogenesis) induced by these RTKs and their extracellular ligands (Gas6, GDNF, and FGF) through either PI3K or MAPK signaling pathway. Significantly, we identify FGFR, RET, and MERTK as the first RTKs that can directly interact with and phosphorylate YAP/TAZ at multiple tyrosine residues independent of upstream Hippo signaling, thereby activating their functions in tumorigenesis. In conclusion, we have identified several novel kinases and extracellular stimuli regulating the Hippo pathway. Our findings also highlight the pivotal role of the Hippo pathway in mediating Gas6/GDNF/FGF-TAM/RET/FGFR-MAPK/PI3K signaling during tumorigenesis and provide a compelling rationale for targeting YAP/TAZ in RTK-driven cancers.

Introduction

The Hippo pathway is an emerging signaling pathway that plays critical roles in various biological processes such as organ size control, tissue homeostasis, tumorigenesis, metastasis, immune response, and mechanotransduction [1–6]. It consists of a large network of protein–protein interactions (PPIs), with at least 35 known components having been identified in *Drosophila* and human to date. The core signaling cascade is comprised of: the serine/threonine (S/T) kinases Warts [7] (Wts) and Hippo [8], scaffold/adapter proteins Salvador [9] (Sav) and Mats[10], and the transcriptional coactivators YAP and its paralog TAZ [11–14]. Hippo, Wts, Sav, and Mats in *Drosophila* are conserved proteins and homologous to mammalian MST1/2, LATS1/2, WW45, and MOB1, respectively [12, 15]. The core components and upstream effectors of the Hippo pathway show a high degree of similarity between *Drosophila* and mammals, implying an evolutionarily conserved, central role in regulating various cellular processes. In mammals, upon activation by upstream stimuli, MST phosphorylates LATS, Sav, and MOB1, which causes complex formation and full activation of LATS kinases. Activated LATS subsequently phosphorylates the oncoproteins YAP and TAZ at five or four different conserved HXR/H/KXXS/T motifs, respectively, including S127 in YAP and S89 in TAZ [11–14]. LATS-dependent phosphorylation of YAP at S127 (pS127) or TAZ at S89 (pS89) produces an interaction site for phosphoprotein-binding protein 14-3-3, which inhibits YAP/TAZ nuclear localization, prevents

Supplementary information The online version of this article (https://doi.org/10.1038/s41388-019-0988-y) contains supplementary material, which is available to authorized users.

✉ Xiaolong Yang
yangx@queensu.ca

[1] Department of Pathology and Molecular Medicine, Queen's University, Kingston, ON K7L 3N6, Canada

Published online: 02 September 2019

interaction with transcription factors such as TEAD, and suppresses transcription of genes involved in promotion of cell proliferation and tissue growth (e.g., CTGF, AREG, and CYR61 [16]). Although several regulatory factors [actin dynamics, cell matrix stiffness, cell–cell contact, and lysophosphatidic acid (LPA)] of the Hippo pathway have been identified within the past 10 years, our understanding of how the Hippo pathway is regulated in response to various extracellular stimuli is certainly incomplete. In addition, the upstream kinase regulators of the Hippo pathway remain largely unknown. Indeed, only a limited number of protein kinases (e.g., EGFR, ERBB4/HER4, and VEGFR) have been identified as upstream regulators of the Hippo pathway [17, 18].

Receptor tyrosine kinases (RTKs) are a family of ligand-binding cell surface receptors that mediate intercellular communication and orchestrate a wide range of essential cellular activities such as cell proliferation, differentiation, survival, metabolism, and migration in response to extracellular cues such as growth factors [19, 20]. Mutations or aberrant activation of many RTKs, such as EGFR and HER2, are causally linked to the development of cancers including breast and lung cancer, which makes them obvious candidates for targeted cancer therapy [21]. In many cancers, dysregulated RTKs are coexpressed with their ligands (e.g., EGFR, PDGFR, and FGF and its receptor (FGFR)) [22]. Currently, there are 58 RTKs in the human kinome, which mediate signals initiated by an even greater number of extracellular stimuli [23]. However, only a few of these RTKs have been shown to be upstream regulators of the Hippo pathway [17, 18]. Whether augmented Hippo signaling is a rare or common mechanism by which RTKs exert their functions is largely unknown.

We have recently reported our development of a LATS biosensor (LATS-BS) that can accurately quantify LATS kinase activity by a split luciferase assay [24, 25]. The LATS-BS consists of 15 amino acids of YAP (YAP15) surrounding the S127 LATS phosphorylation site fused with N-terminal luciferase (YAP15-S127-NLuc) and the phosphorylated YAP (YAP-pS127) binding protein 14-3-3 fused with C-terminal luciferase (14-3-3-CLuc) (Fig. 1a). We tested the utility of this biosensor in vitro and in vivo and used it to identify VEGFR as a novel regulator of the Hippo pathway [24, 25]. Specifically, we found that VEGFR inhibits MST and LATS through PI3K/MAPK signaling and showed that YAP/TAZ are essential for VEGF-induced angiogenesis. While compelling, this previous work offered limited insight into whether other RTKs elicit their effects through augmenting Hippo signaling. In the present study, we aimed to better address this question by performing a systematic functional screen using the LATS-BS and an RTK expression library. We show that many RTKs regulate the Hippo pathway through PI3K or MAPK when activated by their ligands and that the Hippo pathway is the central mediator of several tumorigenic functions of these RTKs including cell proliferation, anchorage-independent growth, cell motility, as well as angiogenesis. Interestingly, we show for the first time that a small number of RTKs, such as FGFR, can directly regulate YAP/TAZ by interacting with and phosphorylating them at tyrosine residues. These findings provide compelling evidence that the Hippo pathway is central in ligand/RTK-initiated aberrant cancer cell signaling and may provide new directions for further development of targeted cancer therapy.

Results

RTKs are common upstream regulators of LATS, YAP, and TAZ

In 2011, Yang et al. developed a library consisting of 558 distinct human kinases and kinase-related protein open reading frames (ORFs) in a pDONR-223 Gateway® entry vector [26]. This library was used to generate an RTK overexpression library by subcloning individual RTK ORFs into a myc-tagged destination expression plasmid through Gateway® Technology cloning as described [27] (Supplementary Fig. 1A). The RTK overexpression library was used to identify upstream RTK regulators of the Hippo pathway through two parallel screens. In the first screen, RTKs were coexpressed with the LATS-BS (indicator of LATS activity by quantifying YAPS127 phosphorylation) in HEK293 cells and biosensor activity was measured through luciferase assays. In the second screen, the activity of an STBS-Luc reporter (indicator of YAP/TAZ co-transcriptional activity through TEAD; Supplementary Fig. 1B) [28] was quantified upon coexpression with each RTK. RTKs regulating the Hippo pathway were defined as those inducing a statistically significant change in reporter activity (>2-fold for LATS-BS or >1.5-fold for STBS-Luc reporter) (Fig. 1b). The results of these screens are summarized in Supplementary Tables 1 and 2 for LATS-BS and STBS-Luc reporter, respectively. Four RTKs activated the LATS-BS, whereas 28 RTKs suppressed its activity (Supplementary Table 1). Thirty-six RTKs activated the STBS-Luc reporter and, interestingly, no RTKs were found to suppress this reporter's activity (Supplementary Table 2). Consistent with canonical Hippo signaling, most RTKs had opposite effects on the LATS-BS (LATS) and STBS-Luc (YAP/TAZ) activities (Fig. 1c, d). From the top candidate Hippo regulators, TAM family members (TYRO3, AXL, and MERTK), RET, and FGFR1/2 RTKs were selected for further characterization based on their novelty, fold-change

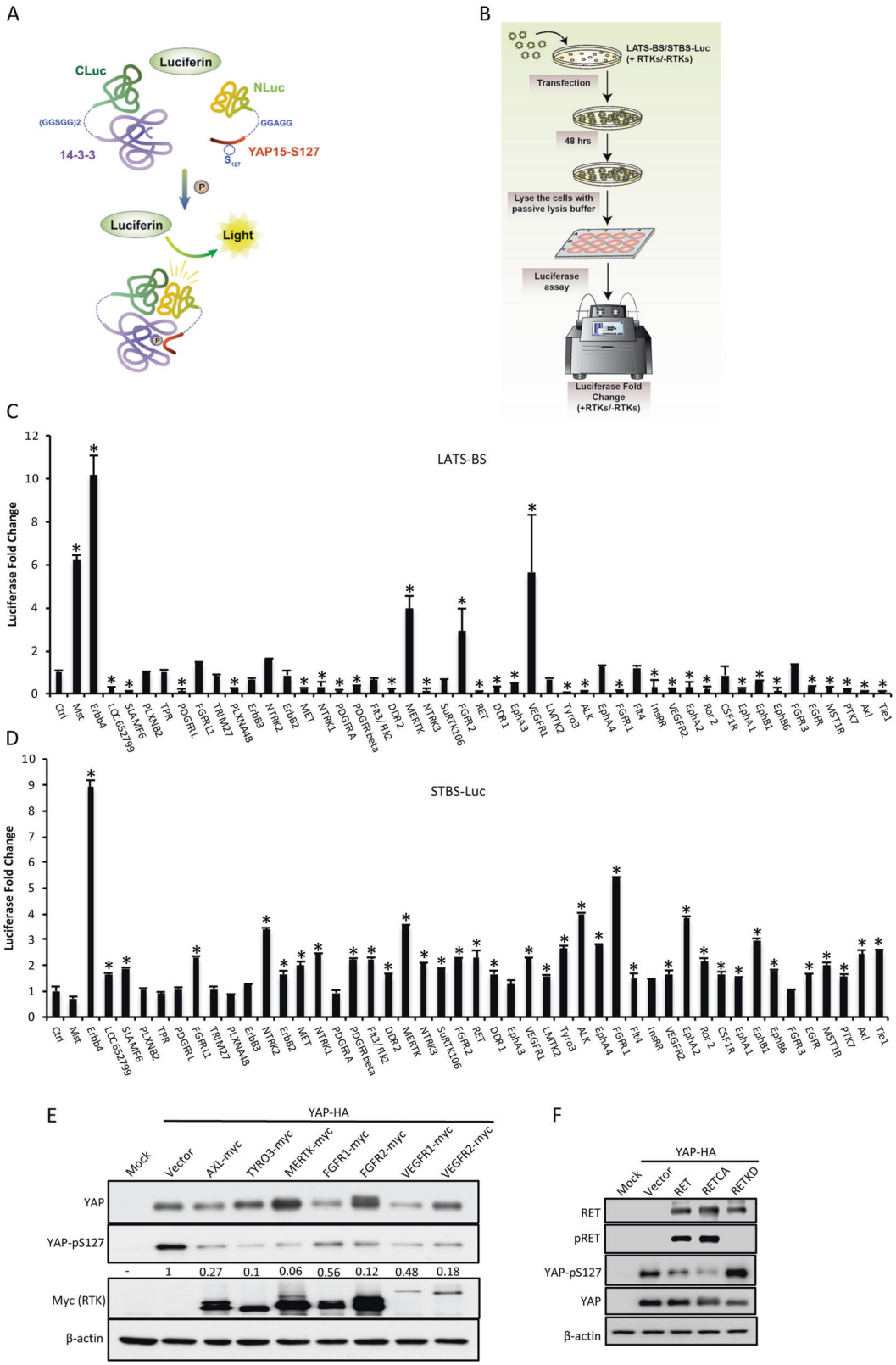

values, and known importance in tumorigenesis. Consideration was also given to the patterns observed across the screens. Interestingly, some RTKs, such as FGFR2 and MERTK, caused simultaneous LATS and YAP activation, suggesting some type of noncanonical Hippo signaling or feedback mechanism might be at play.

◀ **Fig. 1** Parallel screens for RTK regulators of the Hippo pathway using the LATS-BS or STBS-Luc reporters. **a** Schematic diagram of the LATS-BS. When NLuc-YAP15 is unphosphorylated, there is no interaction between YAP15 and 14-3-3; thus, the LATS-BS shows minimal bioluminescence activity. However, phosphorylation of YAP15-S127 by LATS leads to 14-3-3 binding, luciferase complementation, and high biosensor signal. **b** Schematic diagram showing functional screening. HEK293 cells were transfected with LATS-BS or STBS-Luc reporter alone or together with each RTK. 48 h after transfection, luciferase assays were performed. Screening of LATS-BS (**c**) and STBS-Luc reporter (**d**) assay against RTK library. Candidate Hippo pathway regulators were defined as having any statistically significant fold-change value greater than 2 for LATS-BS and 1.5 for STBS-Luc ($n = 2$). **e**, **f** Validation of candidate RTKs regulating the Hippo pathway. Phosphorylation of YAP-S127 was suppressed after transfection with candidate RTKs. Numbers underneath of YAP-pS127 blot in **e** correspond to the normalized phosphorylated/total protein expression (YAP-pS127/YAP) levels. RET and RET-CA (RET constitutive active-M918T) suppresse YAP phosphorylation (YAP-pS127) while kinase-dead RET-KD (RET kinase-dead-K758M) cannot (**f**). Data are represented as mean ± SD

As a validation of the screening results, YAP-S127 phosphorylation was suppressed when YAP was transfected alongside TAM, FGFR1/2 or RET into HEK293 (Fig. 1e, f). As shown previously, VEGFR1/2 suppressed YAP-S127 phosphorylation [24] and was used as a control. Interestingly, YAP stabilization was observed when increasing amounts of MERTK, VEGFR1 and FGFR2 were transfected with a constant amount of YAP (Supplementary Fig. 1C–E).

YAP/TAZ are critical for TAM receptor family activation of cell proliferation and anchorage-independent growth

In order to validate the TAM receptor family as novel upstream regulators of LATS, YAP, and TAZ, we first tested whether activation of TAM receptors with their ligand, Gas6, regulates Hippo pathway transcriptional outputs. Gas6 treatment stimulated endogenous mRNA expression of the YAP/TAZ transcriptional target *CYR61* in TAM-negative MCF10A mammary cells stably overexpressing TYRO3, AXL, or MERTK while the TAM inhibitor LDC1267 reversed this effect (Fig. 2a–c). As a control, Gas6 treatment has no effect on *CYR61* or another YAP/TAZ target, *CTGF*, levels in MCF10A in the absence of the TAMs (Supplementary Fig. 2A). Similar upregulation by these RTKs was also observed for other Hippo downstream targets such as *CTGF* and *ITGB2* (Supplementary Fig. 2B–D). As YAP/TAZ are sequestered in the cytoplasm after phosphorylation by LATS and translocated into the nucleus when LATS is inactivated [11], YAP and TAZ subcellular localization was examined after Gas6 treatment in MCF10A-AXL mammary and MDA-MB-231 breast cancer cells. YAP and TAZ were translocated into the nucleus within 15–60 min of Gas6 treatment (Fig. 2d, e, Supplementary Fig. 2E–H). Upstream of YAP/TAZ, Gas6 treatment in AXL-high Hs.578T and MDA-MB-231 breast cancer, and HeLa cervical cancer cells inhibited LATS kinase activity (as measured by LATS autophosphorylation) and activated YAP/TAZ (reduced inhibitory YAP-S127 and TAZ-pS89 phosphorylation), which could be inhibited by AXL inhibitor (Fig. 2f, Supplementary Fig. 3A, B). Collectively, these data suggest that Gas6/TAM inhibits LATS, allowing enhanced nuclear localization of YAP/TAZ and thereby increasing their transcriptional coactivation functions.

Different RTKs can signal through shared intracellular pathways, yet affect different outcomes. While the mechanisms underlying this remain unclear, this is thought to be due to subtle differences in kinase activity and adapter proteins comprising the multimeric complexes that broadcast signaling [29]. We next explored whether the Hippo pathway effectors contribute to specific biological functions induced by distinct RTKs. Since previous studies show that Gas6 can induce cell proliferation and anchorage-independent growth by binding to and activating TAM RTKs [30–32], we first investigated whether Hippo signaling is critical in mediating this aspect of Gas6/TAM function. We knocked down YAP/TAZ using siRNAs in MCF10A-AXL/TYRO3/MERTK, and TAM-high MDA-MB-231, Hs578T, and HeLa cells. Cell proliferation was assessed after stimulating the cells with Gas6. Gas6 treatment increased cell proliferation in all cell lines. However, knockdown of YAP and TAZ by siRNAs completely abolished Gas6-induced cell growth (Fig. 2g, Supplementary Fig. 3C–G). Interestingly, we also found that knockout of TAZ alone but not YAP by CRISPR was sufficient to suppress Gas6-induced anchorage-independent growth on soft agar in MDA-MB-231 cells (Fig. 2h, i; Supplementary Fig. 3H, I). Moreover, we constructed siYAP/siTAZ-resistant constitutively active mutant YAP/TAZ constructs and performed rescue experiments for cell proliferation (Supplementary Fig. 4A, B) as well as tube formation assay (Supplementary Fig. 4C–E). Addback of YAP and TAZ was sufficient to restore cell proliferation and tube formation. We also performed rescue experiments for the colony formation assay after making CRISPR-resistant addback constructs expressed in stable cell lines (Supplementary Fig. 4F–H). In these experiments, wild-type TAZ but not TAZ-F52/53A, a TAZ mutant lacking interaction with the TEAD transcription factor, could rescue suppressed transformation by TAZ knockout in the presence of Gas6 (Supplementary Fig. 4F–H).

YAP/TAZ are critical for GDNF/RET-induced increased cell proliferation and migration

In fetal development, activation of RET by its ligand GDNF promotes cell proliferation and motility/migration, which

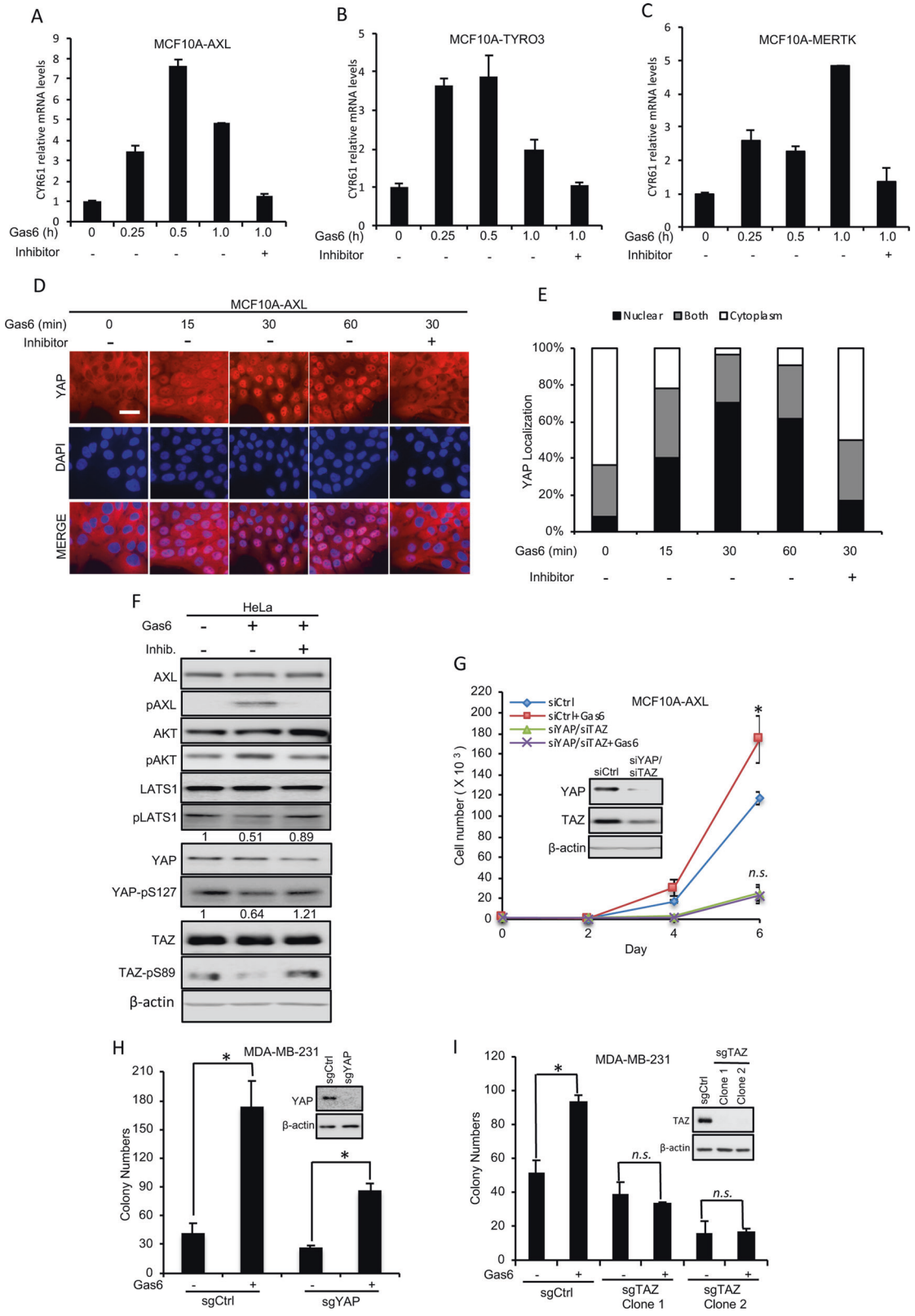

play important roles in the development of the kidneys, nervous, and neuroendocrine systems [33]. In addition, it has been shown that GDNF/RET signaling is dysregulated during tumorigenesis, most notably in lung, thyroid, colon, and neuroblastoma cancers [34–37]. Therefore, we investigated whether Hippo signaling is regulated by and

◀ **Fig. 2** AXL activation increases tumorigenicity in vitro through YAP/TAZ. **a–c** Gas6 increases YAP/TAZ transcriptional coactivation of *CYR61* in MCF10A-AXL/TYRO3/MERTK cells. Cells were treated with 200 ng/mL Gas6 for the indicated times. *CYR61* expression was measured by qRT-PCR. Cells were serum-starved for 24 h before ligand treatment. For some samples, cells were pretreated with TAM inhibitor (LDC1267) at 10 μM for 3 h before and during Gas6 treatment ($n = 2$). Data are represented as mean ± SD. **d**, **e** Gas6 stimulation increases YAP nuclear localization in MCF10A-AXL. **d** Representative images of YAP or TAZ immunostaining are shown after treatment with 200 ng/mL Gas6 for the indicated times. **e** YAP subcellular localization was quantified in three separate experiments in which at least 200 cells were examined. Cells were serum-starved for 24 h before ligand treatment. For some samples, cells were pretreated with TAM inhibitor (LDC1267) at 10 μM for 3 h before and during Gas6 treatment. Scale bar represents 15 μm. **f** Gas6 stimulates phosphorylation of AKT and reduces LATS1 phosphorylation. Hela cells were treated with Gas6 for 30 min. AXL was inhibited using 10 μM inhibitor (LDC1267) for 3 h before and during Gas6 treatment. Numbers underneath of p-LATS1 and YAP-pS127 blots represent normalized phosphorylated/total protein expression. **g** Gas6 promotes proliferation of MCF10A-AXL cells. Transient knock down of YAP and TAZ abolishes cell proliferation induction by Gas6 treatment. Western blot analysis was performed 7 days after siRNA transfection to evaluate knockdown efficiency. Cell proliferation was performed in 2% FBS-containing media. Some cells were treated with 200 ng/mL GAS6, as indicated ($n = 3$). **h**, **i** Gas6 treatment increases colony formation of MDA-MB-231 cells in soft agar. **h** Knockout of YAP by CRISPR causes only a slight decrease in MDA-MB-231 colony formation but these cells remain responsive to Gas6 treatment. **i** Two MDA-MB-231 TAZ knockout clones (sgTAZ-1/2) show no response to Gas6 treatment, compared with the control cells (sgCtrl). Cells were grown in media containing 2% FBS in the absence or presence of 200 ng/mL Gas6, as indicated ($n = 3$). Data are represented as mean ± SD

contributes to GDNF/RET-mediated cell proliferation and motility. We established HEK293, A549 (lung) and HCT116 (colon) cell lines overexpressing constitutively active RET (RET-CA; RET-M918T) [38] in a doxycycline (Dox)-inducible system. RET-CA expression after Dox treatment in each of the aforementioned cell lines induced mRNA expression of *CYR61*, whereas treatment with the RET inhibitor vandetanib abrogated both phosphorylation of RET (pRET) and *CYR61* expression (Fig. 3a–c), suggesting that RET can promote transcriptional coactivation by YAP/TAZ. A similar pattern of activation was observed after GDNF treatment in endogenous RET-high SH-SY5Y (neuroblastoma) cells (Fig. 3d). To confirm that RET is indeed critical for GDNF-induced activation of *CYR61* transcription, we generated a RET knockout SH-SY5Y cell line using CRISPR (sgRET) and found that RET ligand GDNF could not induce *CYR61* expression in this cell line (Fig. 3d). Consistent with YAP/TAZ activation, YAP or TAZ was translocated into the nucleus within 30 min of GDNF treatment (Fig. 3e, f). Cell proliferation and motility were assessed after stimulating parental or YAP/TAZ knockdown SH-SY5Y with GDNF. While GDNF stimulated cell proliferation and motility in parental cells, YAP/TAZ knockdown diminished GDNF-mediated cell proliferation and motility in SH-SY5Y (Fig. 3g, h, Supplementary Fig. 5A, B).

Validation of FGFR as upstream regulators of the Hippo pathway

FGFRs regulate many cellular processes. Numerous reports have described dysregulation of FGF/FGFR signaling pathways in cancers through activating mutations, gene copy number amplification, oncogenic fusion, or epigenetic deregulation [39]. FGF signaling has many physiological roles, particularly in angiogenesis. In fact, it is thought that FGF/FGFR is one of the main compensatory signaling pathways when angiogenesis is targeted by anti-VEGFR therapies [40].

FGFR1/2 were among the top candidate Hippo regulators identified in our screens. To validate this relationship, we assessed the effect of FGF on endogenous *CYR61* mRNA expression in multiple cell lines including FGFR-negative MCF10A cells stably overexpressing FGFR1 or FGFR2, and FGFR-positive MDA-MB-134 (breast) and BHE (lung) cell lines, human umbilical vein endothelial cells (HUVEC), and human blood outgrowth endothelial cells (BOEC). FGF enhanced *CYR61* expression in each of the models tested, which can be blocked by FGFR inhibitors (Fig. 4a, Supplementary Fig. 5C, D). Interestingly, among different FGFs, FGF2 has the most dramatic effect on CYR61 (Supplementary Fig. 5E). Consistent with enhanced endogenous *CYR61* mRNA expression, FGF stimulation decreased LATS phosphorylation (pLATS-T1079), and reduced relative YAP phosphorylation at S127 and TAZ phosphorylation at S89 in BHE cells (Fig. 4b) and YAP/TAZ nuclear translocation in various cell lines (Fig. 4c, d, Supplementary Fig. 6A, B), suggesting that FGF/FGFR activates YAP/TAZ through enhancement of their nuclear localization by inhibiting LATS.

We next investigated the contribution of Hippo signaling to FGF/FGFR-mediated angiogenesis in vitro using a tube formation assay. Pharmacological inhibition of YAP/TAZ with 100 nM of verteporfin (VP) inhibited FGF-induced tube formation by HUVEC cells (Fig. 4e). A similar result was achieved by knockdown of TAZ or YAP in HUVEC cells using siRNA (Fig. 4f–h). Interestingly, TAZ knockdown had a more substantial effect on blocking FGF-induced tube formation than YAP knockdown (Fig. 4g, h, Supplementary Fig. 5F). Addback of YAP/TAZ into the siYAP/TAZ knockdown cells rescued tube formation in the presence of FGF (Supplementary Fig. 4D, E). Pharmacological inhibition of YAP/TAZ using VP also decreased endothelial cell sprouting area in an aorta ring model in a dose-dependent

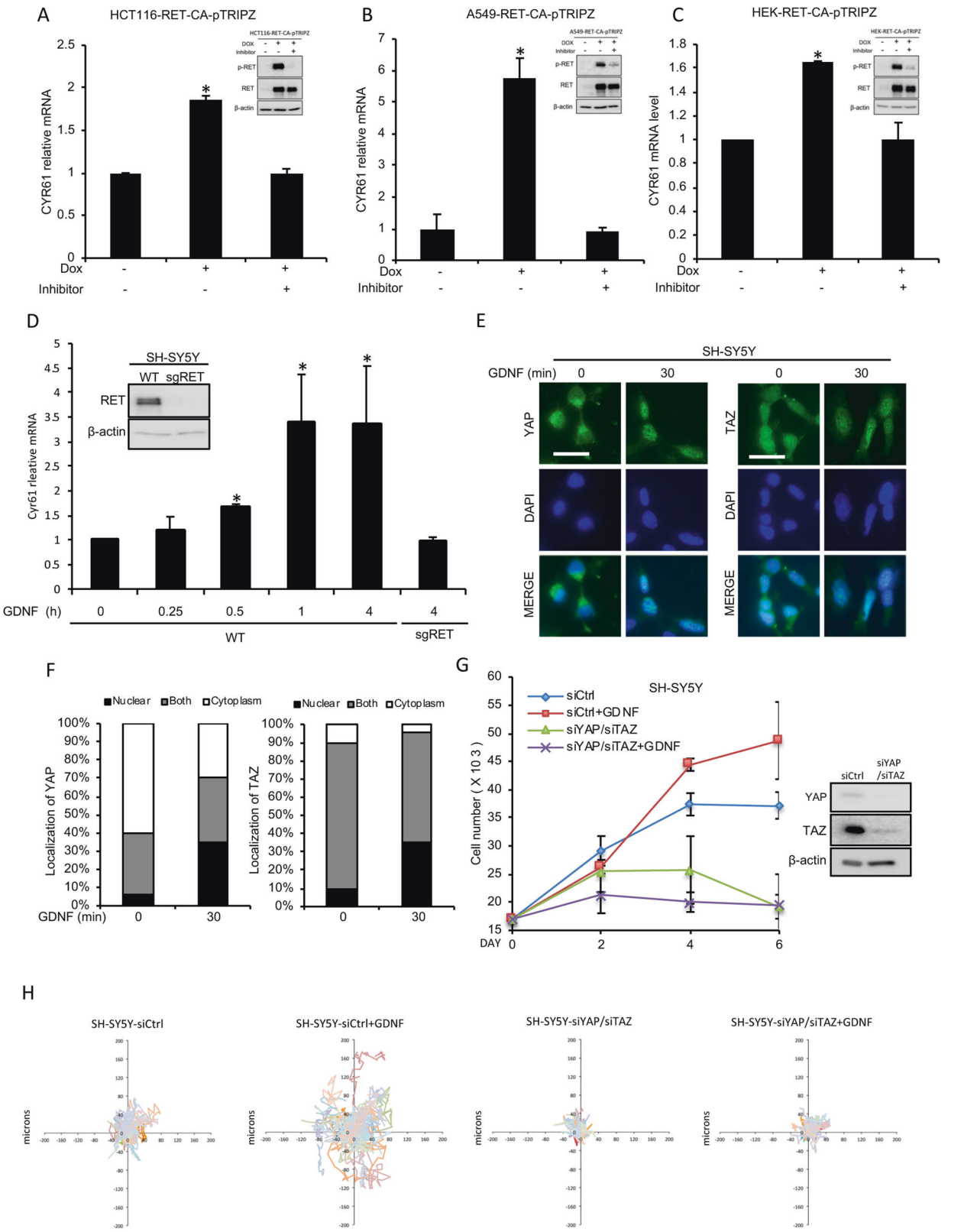

manner (Fig. 4i). As a control, immunofluorescent staining of the aortic sections for an endothelial cell marker, VE-cadherin, confirmed that the observed sprouts represent endothelial cell growth (Supplementary Fig. 5G). Therefore, the Hippo pathway acts downstream of FGF/FGFR to regulate angiogenesis.

◀ **Fig. 3** Knock down of YAP/TAZ suppresses GDNF/RET-induced cell motility in vitro. **a**–**c** Overexpression of a constitutively active RET mutant (M918T) using a Dox-inducible system increases YAP/TAZ transcriptional coactivation of *CYR61* in HCT116, A549 and HEK293 cells, which can be inhibited by a RET inhibitor, vandetanib. To induce RET, cells were treated for 24 h with 1 ug/mL doxycycline in the absence or presence of vandetanib at 1 μM ($n = 2$). Western blot analysis was performed using anti-RET and anti-pRET antibodies. **d** RET-dependent induction of *CYR61* by GDNF in SH-SY5Y. RET was knocked out by sgRET in SH-SY5Y cells. Wild-type (WT) or sgRET SH-SY5Y cells were treated with 100 ng/mL GDNF for indicated times ($n = 2$), followed by qRT-PCR analysis of *CYR61* mRNA. **e**, **f** GDNF stimulation increases YAP/TAZ nuclear localization in SH-SY5Y cells. **e** Representative images of YAP or TAZ immunostaining after treatment with 100 ng/mL GDNF for the indicated times. Scale bars represent 15 μm. **f** YAP/TAZ subcellular localization was quantified in three separate experiments in which at least 200 cells were examined. **g** YAP/TAZ knock down suppresses GDNF-induced cell proliferation in SH-SY5Y cells. Cells were cultured in 2% FBS-containing media during the assay. Western blot analysis was performed 7 days after siRNA transfection ($n = 3$). Data are represented as mean ± SD. **h** YAP/TAZ knock down suppresses GDNF-induced cell motility in SH-SY5Y. Treatment of SH-SY5Y cells transfected with control siRNA (siCtrl) with GDNF (+GDNF) increases cell motility, which can be blocked by transient knockdown of YAP/TAZ ($n = 50$)

Regulation of the Hippo signaling pathway by RTKs through PI3K and MAPK

Previous studies have shown that RTKs exert their functions mainly through PI3K-PDK1-AKT and/or RAF1-MEK-ERK signaling pathways [41, 42]. Interestingly, we and others have reported that RAF1/ERK or PI3K/PDK1 can also regulate the Hippo pathway [43, 44]. To address whether PI3K or MAPK link RTKs with Hippo signaling, MCF10A cells expressing AXL or FGFR1 were stimulated with their respective ligands (Gas6 and FGF) in the absence or presence of inhibitors of PI3K/PDK/AKT, RAF1/MEK, or AXL/FGFR, followed by immunostaining for YAP subcellular localization. VEGFR2-overexpressing cells were included as a positive control. Interestingly, Gas6/AXL increased YAP nuclear translocation mainly through the PI3K-PDK1 pathway and was independent of AKT activity (Fig. 5a), whereas FGF/FGFR and VEGF/VEGFR enhanced YAP nuclear localization through RAF1 (Fig. 5b, Supplementary Fig. 6). In addition, as shown in Fig. 5c, PI3K, PDK, and AXL inhibition all suppressed LATS dephosphorylation in the presence of Gas6, which is consistent YAP/TAZ exclusion from the nucleus. Similarly, RAF inhibition suppressed LATS dephosphorylation in the presence of FGF as well as YAP cytoplasmic sequestration (Fig. 5d). These results provide compelling preliminary evidence that AXL, FGFR, and VEGFR regulate the Hippo pathway through differing molecular mechanisms.

FGFR and YAP directly interact in vivo

It has been reported that the truncated form of the ERBB4 RTK activates YAP through direct interaction [45]. In our screen, we wondered whether other RTKs might directly interact with Hippo pathway components to affect their function. We evaluated the interaction of YAP with FGFR, an RTK that shares significant homology to ERBB4. Surprisingly, co-immunoprecipitation experiments showed a direct interaction between YAP and constitutively active FGFR1 (FGFR-CA) (Fig. 6a). In order to explore whether a direct interaction might exist between FGFR and YAP when expressed at endogenous levels, we developed a novel split luciferase essay called NanoLuc Binary Technology (NanoBiT, Promega) to construct a bioluminescent biosensor detecting the FGFR-YAP PPI and confirmed this interaction using the biosensor. Mechanistically, this system allows for detection of PPI interactions at endogenous levels due to the extreme brightness of NanoLuc luciferase (>200-fold stronger than firefly luciferase) protein. Similar to the LATS-BS, to construct the NanoBiT YAP-FGFR biosensor, NanoLuc luciferase is split into two fragments, LgBiT and SmBiT, which are linked to YAP and FGFR, respectively. Interaction of YAP and FGFR in cells will bring LgBiT and SmBiT in proximity, resulting in their complementation and subsequent light emission (Fig. 6b). A weak HSV-TK promoter is used to express each construct, achieving expression levels of YAP-LgBiT and FGFR-SmBiT that are comparable to endogenous protein levels in cells. Using this YAP-FGFR biosensor, we confirmed a theoretical direct interaction could occur between YAP and FGFR1 or FGFR2 when expressed at endogenous protein levels (Fig. 6b). Thus, the interactions that we have described between YAP and FGFR are unlikely to be caused by protein overexpression and nonspecificity. We next performed a co-IP to confirm the existence of a bona fide interaction between YAP and FGFR in vivo using endogenous proteins extracted from BHE cells. Significantly, we showed a strong interaction between endogenous YAP and FGFR after FGF treatment, which can be inhibited by FGFR inhibitor but that was enhanced after LATS1/2 knockdown (Fig. 6c). Thus, YAP and FGFR1 interact in vivo.

We further examined whether FGFR1 and YAP colocalize in cells. We performed immunostaining of FGFR1 and YAP in the absence or presence of FG and found that YAP is indeed colocalized with FGFR1 in the cytoplasm of BHE cells cultured in serum-starved medium, whereas both YAP and FGFR1 are translocated into the nucleus after FGF treatment (Supplementary Fig. 7A). As an antibody control, western blot analysis of four different cancer cell lines expressing varying levels of FGFR1

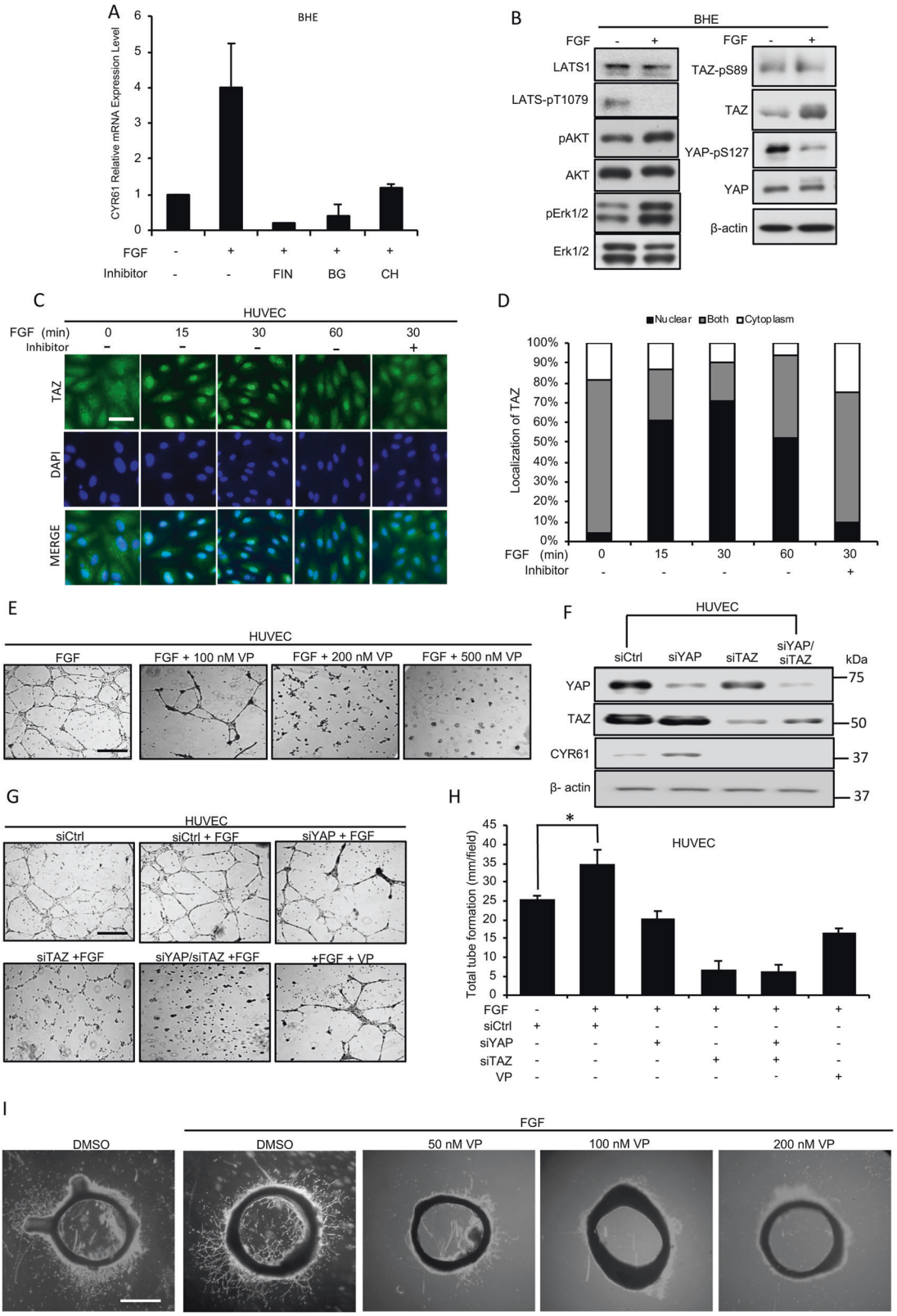

(BHE > MDA-MB231 > MCF7 > MCF10A) were concordant with the immunostaining results when the same exposure time was used across images (Supplementary Fig. 7B, C). Thus, YAP and FGFR1 colocalize in cells, which supports our model of a direct interaction between these two proteins in vivo.

◀ **Fig. 4** FGF/FGFR regulates angiogenesis through YAP/TAZ in vitro and ex vivo. **a**, **b** Treatment of cells with FGFR ligand induces YAP/TAZ transactivating function. BHE cells were treated with ligand/inhibitor for different times. Ligand treatments activated YAP/TAZ, while inhibitor treatment prevents activation. **a** *CYR61* expression was measured by qRT- PCR. Some samples were treated with the indicated inhibitors [FIN (FIN-2), BG (BGJ398), and CH (CH5183284)] at 1 μM or/and 200 ng/mL FGF for 24 h ($n = 2$). Data are represented as mean ± SD. **b** FGF stimulates phosphorylation of AKT and ERK1/2 in BHE cells, and reduces YAP and TAZ relative phosphorylation. BHE cells were treated with 200 ng/mL FGF for 24 h. **c**, **d** FGF stimulation increases TAZ nuclear localization in HUVEC cells. **c** representative images of TAZ immunostaining after treatment with 200 ng/mL FGF for the indicated times. Scale bar represents 15 μm. **d** TAZ subcellular localization was quantified in three separate experiments in which at least 200 cells were examined. Some samples were pretreated with FGFR inhibitor AZD4547 at 10 μM for 3 h before and during FGF treatment. **e** Verteporfin (VP) treatment inhibits tube formation by HUVEC. Tube formation assays were performed on HUVEC cells treated with FGF and the indicated concentrations of VP. Representative images are shown. Scale bar denotes 200 μm. **f**–**h** YAP/TAZ are critical for FGF-induced tube formation in HUVEC. **f** YAP and TAZ were transiently knocked down by siRNA in HUVEC cells, which reduced CYR61 expression. **g** Representative images showing Matrigel tube formation assays 48 h after siRNA transfection. For some conditions, cells were stimulated with 200 ng/mL FGF or were treated with 100 nM VP for the duration of the tube formation assay. Scale bar denotes 200 μm. Total tube formation was quantified in **h** ($n = 3$). **i** Inhibition of YAP/TAZ using VP reduces angiogenesis ex vivo in a rat aorta model. Sections of aorta were cultured in Matrigel for one week with 200 ng/mL FGF and the indicated concentrations of VP. Scale bar denotes 500 μm

YAP and TAZ are tyrosine phosphorylated by FGFR1/2

Interestingly, while investigating the direct interaction between FGFR1 and YAP, we observed that treatment of BHE cells with FGF, or coexpression of YAP with FGFR1-CA, caused YAP to migrate at an increased molecular weight on SDS-PAGE electrophoresis ("band shift") (Fig. 6d). This finding raised the intriguing possibility that FGFR could cause changes in YAP phosphorylation status, perhaps through direct phosphorylation. To investigate if the band shift is caused by FGFR tyrosine phosphorylation of YAP, we co-transfected YAP alongside FGFR1-CA, FGFR2, or kinase-dead FGFR1 (FGFR1-KD), and assessed for YAP tyrosine phosphorylation using an anti-phosphotyrosine (pY) antibody. YAP was tyrosine phosphorylated when co-transfected with FGFR1-CA or FGFR2 but not with FGFR1-KD (Fig. 6e, Supplementary Fig. 7D, E). Similar to its paralog, tyrosine phosphorylation was also detectable when TAZ was co-transfected with FGFR2 (Supplementary Fig. 7F). To investigate whether FGFR-induced YAP tyrosine phosphorylation occurs independent of the upstream Hippo signaling, we co-transfected FGFR1-CA into HEK293 alongside YAP-5SA, a Hippo-independent YAP mutant in which the five LATS serine phosphorylation residues are mutated to alanine (5SA). Indeed, FGFR1-CA was still able to induce tyrosine phosphorylation of this mutant construct suggesting that this occurs independent of LATS (Fig. 6c). Consistent with this, knockdown of LATS1/2 with siRNAs or by CRISPR could not block the YAP tyrosine phosphorylation FGF or FGFR1-CA (Fig. 6c, Supplementary Fig. 7G).

We next tested whether FGFR can directly phosphorylate YAP through in vitro kinase assays using purified constitutively active truncated form of FGFR1 or FGFR2 and a YAP/GST-fusion protein. FGFR1 and FGFR2 directly phosphorylated YAP-GST in vitro (Fig. 6g, Supplementary Fig. 8A, B). Tyrosine phosphorylation of YAP by FGFR1 or FGFR2 was detectable in a fragment of YAP encompassing amino acids 300-500 (YAP-300-500) (Supplementary Fig. 7H). Closer inspection of this region revealed only three tyrosine residues (Y391, Y407, and Y444) in YAP and two (Y305 and Y321) in TAZ (Fig. 7a, b). In vitro kinase assays showed that all three of these YAP residues are phosphorylated by FGFR1/2 (Fig. 6g, Supplementary Fig. 8B). Consistent with YAP, TAZ can also be phosphorylated by FGFR on the conserved Y305 and Y321 sites in vitro and in vivo (Supplementary Fig. 8C, D).

To further confirm this observation, we created mutant forms of YAP in which all tyrosine residues are mutated to phenylalanines (YAP-6YF) with single tyrosine residues left unmutated (YAP-5YF-188Y, −247Y, −248Y, −391Y, −407Y, and −444Y). These six mutated YAP constructs, each with a single available tyrosine, were co-transfected with myc-tagged FGFR1-CA into HEK293 cells and tyrosine phosphorylation of YAP was assessed. FGFR1-CA phosphorylated YAP-5YF-Y391 and −Y444 (Fig. 6h). Although Y407 tyrosine phosphorylation was detectable in vitro in kinases assays (Fig. 6g) but not in vivo (Fig. 6h), phosphorylation of Y407 in YAP (YAP-pY407) was detectable in full length YAP using a commercially available antibody against phosphorylated Y407 (Fig. 6h). This finding suggests that phosphorylation of Y391 and/or Y444 may be required for Y407 phosphorylation of YAP in vivo. We confirmed the specificity of the anti-YAP-pY407 antibody by measuring tyrosine phosphorylation of YAP-Y407 by constitutively active c-Abl-Δ1-81, which has been previously reported to phosphorylate YAP at Y407 [46] (Supplementary Fig. 9A).

To validate whether FGFR causes YAP phosphorylation under physiological conditions, we evaluated the tyrosine phosphorylation of endogenous YAP/TAZ after FGF ligand treatment in FGFR-positive BHE lung cancer cells. FGF treatment caused endogenous YAP tyrosine phosphorylation in this cell line (Fig. 6i). Thus, endogenous YAP is tyrosine phosphorylated in the presence of FGF. Recently, non-RTKs c-ABL and Src family members (e.g., SRC and LCK) have been found to phosphorylate YAP/TAZ on tyrosine residues [47–49]. To confirm

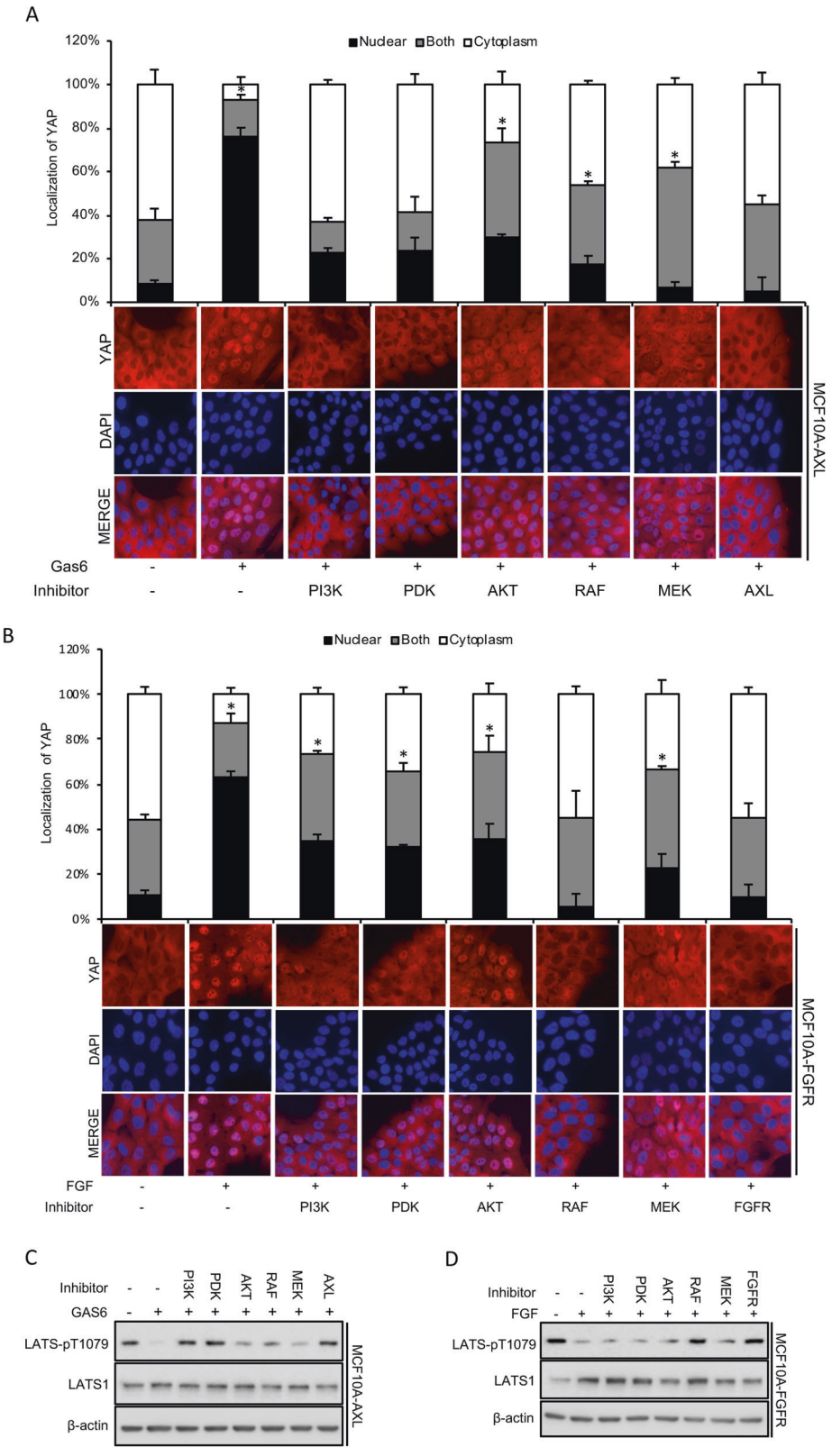

Fig. 5 FGFR and AXL regulate YAP nuclear localization through PI3K and MAPK signaling pathways. MCF10A cells, stably expressing AXL (**a**) or FGFR (**b**) were treated with ligand/inhibitor as indicated. MCF10A-AXL or FGFR1 cells were pretreated with the following inhibitors for 3 h before and during ligand treatment: PDK inhibitor (GSK2334470), PI3K inhibitor (LY294002), AKT inhibitor (Triciribine), RAF inhibitor (LY3009120), or MEK inhibitors (PD98059) ($n = 3$). **c**, **d** Western blot analysis of LATS1 and its phosphorylation (pLATS-T1079) in the presence of ligands/inhibitors treated with the same experimental conditions as **a** and **b**

that FGFR-induced YAP tyrosine phosphorylation was not indirectly mediated through these kinases, we performed several experiments. First, we examined YAP tyrosine phosphorylation after overexpression of YAP-WT, YAP-5YF-391Y, YAP-5YF-Y407, and YAP-5YF-Y444 with constitutively active mutant c-ABL(Δ1-81).

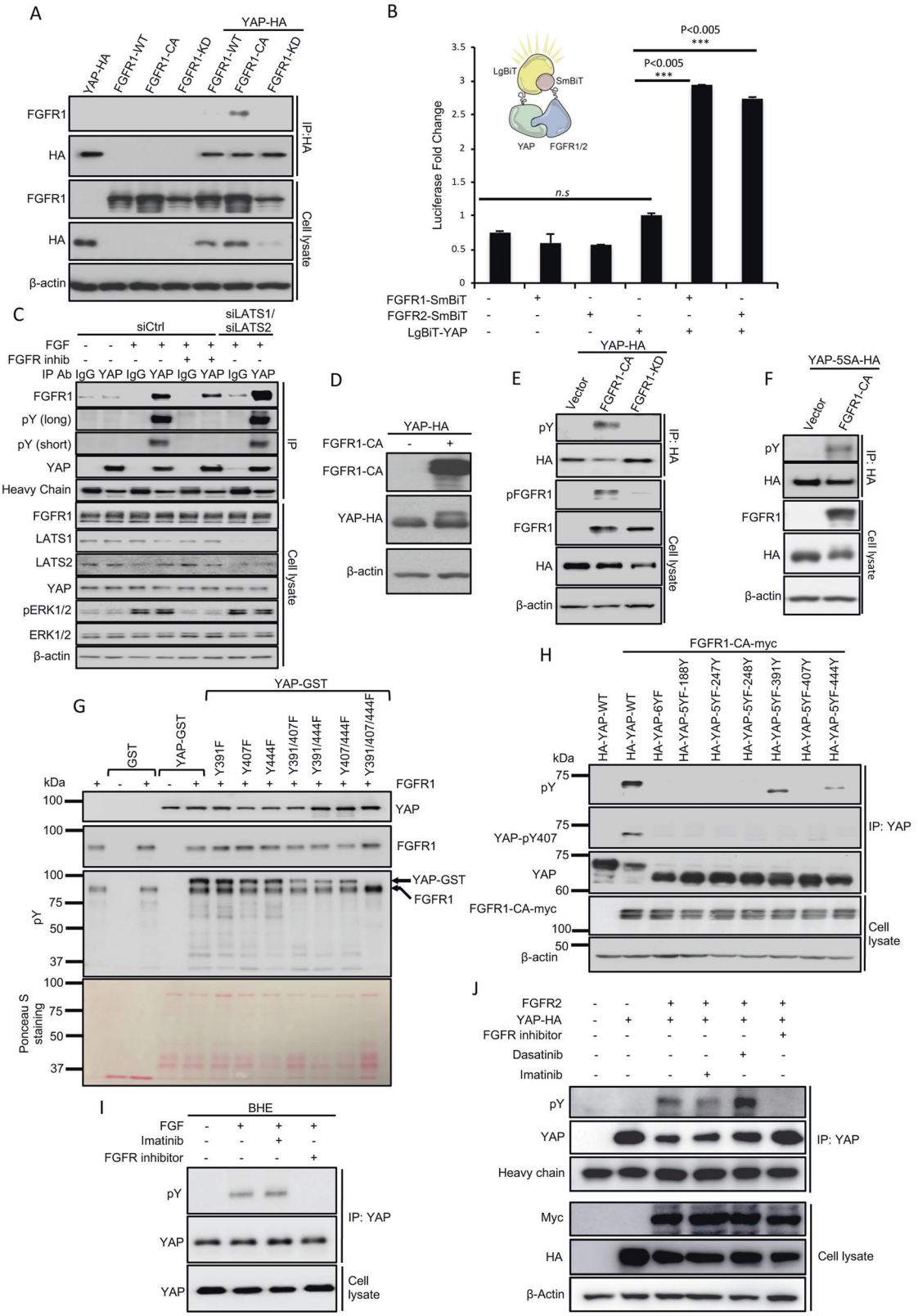

As previously described, c-ABL did phosphorylate YAP on Y407 (Supplementary Fig. 9A). However, it was unable to phosphorylate the Y391 or Y444 residues. Therefore, the YAP phosphorylation patterns observed with c-ABL and FGFR differ, suggesting it is unlikely that FGFR phosphorylates YAP via c-ABL alone. Second,

◀ **Fig. 6** FGFR regulates YAP through tyrosine phosphorylation. **a** FGFR1-CA interacts with YAP. Western blot analysis showing co-immunoprecipitation of FGFR1-CA (K654E) with YAP-HA. YAP-HA plasmid was transfected into HEK293 cells with or without WT, CA (K654E), or kinase-dead (K514A) FGFR1. **b** Proof-of-principle for an endogenous FGFR-YAP interaction using the NanoBiT biosensor. Using the NanoBiT, SmBiT, and LgBiT luciferase fragments were fused respectively to FGFR1-CA/FGFR2 and YAP in a plasmid with HSV-TK promoter. The YAP-LgBiT and FGFR1/2-SmBiT plasmids were transfected alone or together into HEK293 cells ($n = 3$). After 48 h, luciferase assays were performed. The fold changes of luciferase activity for each transfected cells compared with untransfected control cells were calculated. The mean and standard deviation of three samples were shown. Statistical analysis with Student's t test was performed. n.s., no statistical significance ($p > 0.05$); ***, significant ($p < 0.005$). **c** Interaction of endogenous YAP with FGFR1 and tyrosine phosphorylation of endogenous YAP after FGF treatment in BHE cells. BHE cells were untreated or treated with FGF and lysates were immunoprecipitated (IP) with IgG (control) or anti-YAP antibody, followed by western blot analysis of FGFR1 or pY. Similar IP and western blot analysis were performed after LATS1/2 knockdown in BHE cells. Blot with long or short exposure time are shown for pY. Protein lysates were also subjected to western blotting analysis of the levels of FGFR, LATS1, LATS2, YAP, ERK, and pERK. β-actin was used as an internal control. **d** Expression of the FGFR1-CA mutant causes a band shift in coexpressed YAP-HA. **e** Phosphorylation of YAP on tyrosine residues by FGFR1-CA but not kinase-dead FGFR1-KD. YAP-HA plasmid was transfected alone or together with FGFR1-CA-myc or FGFR1-KD-myc into HEK293 cells. YAP-HA was immunoprecipitated, followed by western blot analysis using anti-phosphotyrosine (pY) antibody. **f** HEK293 cells were transfected with Hippo-independent mutant YAP-5SA-HA alone or together with FGFR1-CA. YAP-5SA-HA was immunoprecipitated, followed by western blot analysis using an anti-phosphotyrosine (pY) antibody. **g** YAP tyrosine phosphorylation by constitutively active truncated form of FGFR1 in vitro. GST, YAP-GST wild-type, or YAP-GST tyrosine mutant fusion proteins were incubated at 30 °C with or without purified FGFR1 protein in the presence of ATP. Thirty minutes after incubation, western blot analysis was performed using anti-pY antibody. YAP is tyrosine phosphorylation by FGRR1 on Y391, Y407, and Y444. **h** Mutant YAP constructs with one available tyrosine each were co-transfected alongside FGFR1-CA into HEK293 and were immunoprecipitated for western blot analysis. Tyrosine phosphorylation on YAP-Y391 and Y444 was detectable with a pan anti-pY antibody. Phosphorylation of Y407 was detected only using an antibody specific to this phosphorylation site. **i** FGF treatment causes tyrosine phosphorylation of endogenous YAP. BHE cells were treated with 200 ng/mL FGF for 24 h. For some samples, cells were treated with Imatinib (c-ABL inhibitor) or AZD4547 (FGFR inhibitor) at 1 μM during the ligand treatments. **j** FGFR-induced tyrosine phosphorylation of YAP is not mediated by c-ABL or SRC tyrosine kinase family members. FGFR2 was transfected with YAP-HA and YAP tyrosine phosphorylation was evaluated after immunoprecipitation. Some cells were treated for 24 h with FGFR inhibitor (AZD4547, 1 μM), c-ABL inhibitor (Imatinib, 1 μM), or SRC family inhibitor (Dasatinib, 1 μM). Only the FGFR inhibitor abolished YAP tyrosine phosphorylation

we treated FGFR1-high BHE or HuCCT1 cells with FGF in the absence or presence of a c-ABL inhibitor, Imatinib, or an FGFR inhibitor. As expected, only the FGFR inhibitor was able to inhibit FGF-induced YAP tyrosine phosphorylation (Fig. 6i; Supplementary Fig. 9B). Similarly, Imatinib or a dual c-ABL/SRC inhibitor, Dasatinib, could not suppress YAP tyrosine phosphorylation in the presence of FGFR2 (Fig. 6j). Finally, we overexpressed FGFR1/2 in SRC family member *Src, Yes, Fyn* (*SYF*) knockout mouse embryonic fibroblast cell lines. YAP was still tyrosine phosphorylated by FGFR1 or FGFR2 in *SYF* KO cells (Supplementary Fig. 9C, D). Together, these experiments provide further supportive evidence of our model that FGFR can directly phosphorylate YAP independent of non-RTKs.

FGFR, RET, and MERTK regulate YAP/TAZ through tyrosine phosphorylation

We next explored whether other RTKs can also phosphorylate YAP on tyrosine residues. Interestingly, we found that MERTK and RET also phosphorylated YAP on tyrosine (Fig. 7c). We further performed in vitro kinase assays to identify the sites phosphorylated by RET and found that RET phosphorylates YAP on Y391/Y407/Y444 in vitro (Supplementary Fig. 10A, B). Interestingly, in vivo phosphorylation experiments suggested that both RET and MERTK only phosphorylate YAP on Y444 (Supplementary Fig. 10C–E).

To explore the functional significance of FGFR/RET/MERTK-induced YAP/TAZ tyrosine phosphorylation, we knocked down YAP/TAZ in BHE cells and performed rescue experiments with YAP/TAZ tyrosine phosphorylation-mimetic (YAP-3YE and TAZ2YE) and tyrosine phosphorylation-inactivated (YAP-3YF and TAZ2YF) mutants. To achieve expression levels closer to endogenous YAP/TAZ levels, rescue experiments were performed using transient transfection of the YAP/TAZ constructs into YAP/TAZ knock down (siYAP/siTAZ) BHE cells. YAP-3YE/TAZ2YE or YAP-3YF/TAZ2YF plasmids were modified to generate siRNA-resistant constructs (Fig. 7d). YAP/TAZ tyrosine phospho-mimetic (YE-AB) but not phospho-inactive (YF-AB) addback mutants rescued cell proliferation (Fig. 7e), transformation (Fig. 7f, g), and cell migration (Fig. 7h) phenotypes in YAP/TAZ knock down cells treated with FGF. We also performed the experiment on cell proliferation assay in the absence of FGF (−FGF). Interestingly, our results show that YE-AB, which mimics FGF treatment, causes enhanced cell proliferation (Supplementary Fig. 11). Interestingly, inactivating pY mutant YF-AB rescues the reduced cell proliferation phenotype caused by siYAP/siTAZ just like wild-type YAP, suggesting that inactivation of these Ys alone will not affect basic YAP oncogenic function. Moreover, we generated stable cell lines in MCF10A with Dox-inducible expression of the tyrosine phosphorylation-mimetic YAP/TAZ mutants, YAP-Y444E, YAP-Y391/407/444E (3YE), TAZ-Y304E, TAZ-Y321E, and TAZ-Y304/321E (2YE).

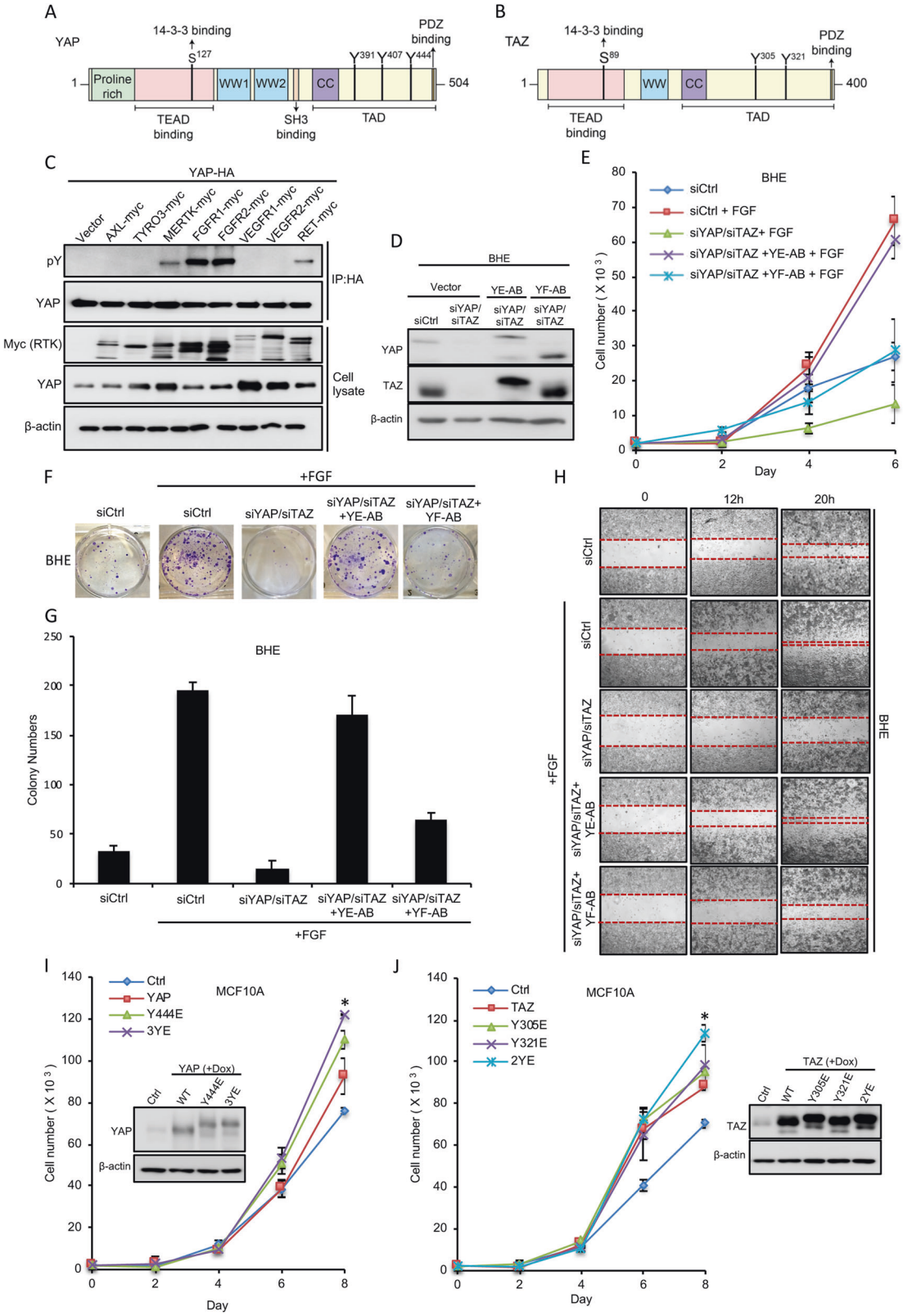

Overexpression of YAP-Y3E or TAZ-Y2E caused enhanced proliferation of MCF10A cells compared with overexpression of wild-type YAP or TAZ (Fig. 7i, j). Together, our findings strongly suggest that direct tyrosine phosphorylation of YAP/TAZ by RTKs such as FGFR, RET, and MERTK may be critical for YAP/TAZ in

◀ **Fig. 7** Several RTKs regulate YAP through tyrosine phosphorylation. Schematic diagram of YAP1 (**a**) and TAZ (**b**) structures reveal potential C-terminal tyrosine phosphorylation sites (Y391, Y407, and Y444 for YAP; Y305 and Y321 for TAZ). **c** Multiple RTKs induce tyrosine phosphorylate of YAP. Candidate RTKs were co-transfected with YAP-HA into HEK293 cells. Forty-eight hours after transfection, protein was harvested and YAP-HA immunoprecipitated. All RTKs-transfected cells were treated with 200 ng/mL of their corresponding ligands for 24 h. **d** Western blot analysis of YAP and TAZ expression. YAP-3YE/TAZ2YE or YAP-3YF/TAZ2YF plasmids were constructed and subsequently modified to generate siRNA-resistant constructs. BHE cells were transfected with siYAP/siTAZ and subsequently transfected with vector, YAP-3YE/TAZ2YE or YAP-3YF/TAZ2YF expression plasmids. The transfection was optimized to achieve high efficiency and comparable expression with endogenous protein levels. **e**–**h** Functional rescue experiments using siRNA-resistant YAP/TAZ constructs. YAP/TAZ tyrosine phosphorylation-mimetic constructs (YE-AB) but not phosphorylation-inactive constructs (YF-AB) are able to rescue the reduced cell proliferation (**e**), colony formation (**f**, **g**), and cell migration (**h**) phenotypes caused by loss of YAP/TAZ (siYAP/siTAZ) in the presence of 200 ng/mL FGF. **i**, **j** Tyrosine mimetic mutations, YAP-Y444E, YAP-Y391/407/444E (3YE), TAZ-Y305E, TAZ-Y321E (2YE), and TAZ-Y305/321E increase cell proliferation in MCF10A cell lines. To induce YAP/TAZ, cells were treated with 1 ug/mL doxycycline during the assay ($n = 3$). Data are represented as mean ± SD

mediating FGF/GDNF/Gas6-induced tumorigenesis and metastasis.

Discussion

Hippo signaling plays a crucial role in development and cancer biology [50]. Although Hippo pathway components have been shown to be important mediators of responses to extracellular stimuli such as TGF-β, LPA, and ligands of G protein-coupled receptors [51, 52], the precise signaling events underlying these and other responses remain unclear. Recently, a few studies have shown a connection between certain RTKs and the Hippo pathway. The Hippo pathway can be regulated by growth factors such as EGF and neuregulin through RTKs such as EGFR family members [18, 24, 45, 53, 54]. We recently demonstrated a novel role for the Hippo pathway downstream of VEGFR in angiogenesis [24, 25]. However, whether Hippo signaling is a common mechanism by which RTKs exert their functions remained unclear. In the present study, we used our LATS activity biosensor [24, 25] and a YAP/TAZ luciferase reporter to perform the first comprehensive gain-of-functional screen for novel RTKs regulating the Hippo pathway. We identified 32 and 36 RTKs regulating the Hippo pathway core components LATS and its substrates YAP/TAZ, respectively. Interestingly, 28 RTKs regulated both LATS and YAP/TAZ, suggesting that the majority of RTKs regulate LATS-YAP/TAZ signaling in the canonical Hippo pathway. We further validated the screening results and provided convincing evidence that the Hippo pathway is a central output of multiple RTKs, including RET, and TAM and FGFR family members, stimulated by their extracellular growth factor ligands GDNF, Gas6, and FGF in important biological functions, such as cell proliferation, anchorage-independent growth, cell motility, and angiogenesis. However, it has also been shown that these RTKs play important roles in many other biological functions. For example, TAM family members have been shown to be involved in the regulation of chemo-resistance, metastasis, and immune homeostasis [51]. Therefore, our observation that the Hippo pathway functions downstream of multiple RTKs may hold even greater significance. Consistent with this notion, although we previously showed that the Hippo pathway is a mediator of VEGFR during angiogenesis, we have now found that the Hippo pathway is critical in mediating VEGF/VEGFR-induced increased cell migration and cell proliferation in breast cancer cells (Supplementary Fig. 12A–K). Therefore, it will be compelling to further explore how the Hippo pathway is involved in other important biological functions of these RTKs in cells. Moreover, in this study, we have validated only six RTKs as novel regulators of the Hippo pathway. Further validation of other candidates as novel RTK regulators of the Hippo pathway will significantly expand our understanding of the crosstalk between the Hippo pathway and RTK signaling in a wide variety of biochemical and biological functions.

In this study, we used our LATS-BS and a YAP/TAZ reporter STBS-Luc to perform two screens in parallel. The two screens showed high overlap between resultant candidates, confirming their validity. However, the observed fold-change values caused by RTK overexpression were significantly higher using the LATS-BS due to its higher sensitivity compared with STBS-luc (Fig. 1c, d; Supplementary Tables 1 and 2). A similar kinome screen by in vitro kinase assay using immunoprecipitated kinases and recombinant LATS was previously performed by Meng et al. who identified MAP4K family S/T kinases as novel kinases phosphorylating LATS [55]. Our screen using the LATS-BS, has several advantages over previous approaches. It can be used to monitor LATS kinase and Hippo signaling activity in real time and in vivo; it has greater sensitivity; and it could reasonably be scaled-up to perform high-throughput screens. Therefore, future large-scale kinome screens using the LATS-BS will undoubtedly identify additional new activators or inhibitors of the Hippo signaling pathway.

In this study, we found that while most RTKs inhibit LATS kinase activity, some RTKs, such as ERBB4, MERTK, FGFR2, and VEGFR1, activate both LATS

kinase and YAP/TAZ transcriptional activating functions in transient luciferase assays (Fig. 1c, d). Interestingly, these RTKs either have the most dramatic effect on YAP/TAZ reporter STBS-luc (e.g., ERBB4 and MERTK) or directly interact with and phosphorylate/activate YAP/TAZ (e.g., MERTK, and FGFR2). Given that it has been reported that overactivation of YAP can subsequently increase LATS kinase activity through a negative feedback pathway [52], this result suggests the possibility of LATS-BS activation through negative feedback when YAP/TAZ is robustly activated by RTKs. Specifically, overexpression of MERTK or FGFR2 stabilizes YAP, causing activation of the STBS reporter (Fig. 1e, Supplementary Fig. 1C, E). Increased YAP activity subsequently may activate a known feedback pathway that upregulates LATS kinase, which would lead to an increase in the LATS-BS signal (Fig. 1c) [56]. Consistent with this, a similar pattern in STBS/LATS-BS activity is observed with a known Hippo regulator, and strong activator of YAP, ERBB4 [45]. Indeed, we have found that overexpression of YAP alone can upregulate LATS kinase activity and the LATS-BS signal in our recently published protocol using the LATS-BS [25].

Activation of RTKs is frequently detected in various cancers and drugs targeting RTKs are widely used for first line or adjuvant cancer treatment. Unfortunately, intrinsic and acquired resistance of cancer patients to single RTK-targeted therapies frequently occurs due to activation of other RTKs or downstream signals from the MAPK/PI3K pathways, which often results in short-term and limited effects on overall survival of patients. While analyzing RTK-induced YAP nuclear localization and activation, we were surprised to find distinct signaling pathways can connect different RTKs to the Hippo pathway. While Gas6-AXL activates YAP/TAZ through the PI3K-PDK1 pathway, independent of AKT activity, FGF/FGFR and VEGF/VEGFR activates YAP/TAZ mainly through activation of RAF1-MEK MAPK pathway (Fig. 5a, b, Supplementary Fig. 6). Our data are the first to show that, although RTKs have very similar kinase domains, they may use distinct signaling pathway to activate the same downstream target, YAP/TAZ. YAP/TAZ-activating RTKs and their ligands, such as AXL and FGF1 [11, 57], are also transcriptionally upregulated by YAP/TAZ, suggesting positive feedback loops could exist between RTKs and YAP/TAZ. Therefore, coactivation of YAP/TAZ and RTKs in cancers may be an important mechanism by which cancer cells could sustain proliferation during tumorigenesis or may escape the antiproliferative effects of RTK-targeted therapies. This finding may provide a preclinical rationale for targeting YAP/TAZ in RTK/MAPK/PI3K-activated or RTK/MAPK/PI3K inhibitor-resistant cancers. Moreover, since crosstalk between RTKs and the Hippo pathway may be important for tumorigenesis and metastasis, combined treatment with RTK- and YAP/TAZ-targeted drugs might provide a useful new therapeutic strategy for successful cancer treatment.

In this study, we identified a new mechanism by which YAP/TAZ are regulated. We provided compelling preliminary evidence that the FGFR/RET/MERTK RTKs can directly phosphorylate YAP/TAZ on tyrosine residues both in vitro, using purified proteins, and in vivo in living cells (Fig. 6−10; Supplementary Fig. 7A–G). It is unclear why these specific RTKs, and not others, can directly phosphorylate YAP/TAZ. Since we found that only constitutively activate FGFR1 (FGFR1-CA) and not its wild-type counterpart directly interacts with YAP in cells (Fig. 6a), we propose that these RTKs have a higher kinase activity than others under these experimental conditions, which may trigger distinct downstream signaling such as direct activation of YAP/TAZ through tyrosine phosphorylation. It will be very interesting to further explore how these RTKs regulate cellular functions through Hippo-LATS-dependent and -independent pathways under different upstream regulatory factors. Moreover, several non-RTKs also phosphorylate YAP and TAZ on tyrosine residues. For example, phosphorylation of YAP on Y407 by c-ABL is a critical step in activation of proapoptotic genes, especially p73, in response to DNA damage [49]. In addition, YAP or TAZ tyrosine phosphorylation by SRC kinase family members, such as SRC, YES, and LCK, has also been reported [48, 58, 59]. However, our studies clearly indicate that FGF/FGFR-induced YAP tyrosine phosphorylation is direct and independent of these non-RTKs. Moreover, by mimicking tyrosine phosphorylation, we have demonstrated that tyrosine phosphorylation of both YAP and TAZ activate its activity in regulating cell proliferation, transformation, and cell migration. Further studies exploring the roles of these tyrosine phosphorylation sites may increase our insight into the molecular mechanism underlying the regulation of YAP/TAZ and Hippo signaling by RTKs in various biological processes. Future work may also identify novel mechanisms of YAP/TAZ regulation by RTKs. Indeed, our observation that FGFR1 is localized to the cell membrane and cytoplasm under serum starvation and to the nucleus with FGF treatment was also somewhat surprising but may point to the existence of an intracellular interaction between FGFR and YAP/TAZ. Indeed, previous studies have reported that FGFR1 can traffic from the cytoplasm to the nucleus after FGF treatment [60–62].

In conclusion, using functional screens, we have identified the Hippo pathway and YAP/TAZ oncoproteins as a central output of various biological processes induced by ligand activation of multiple RTKs and their

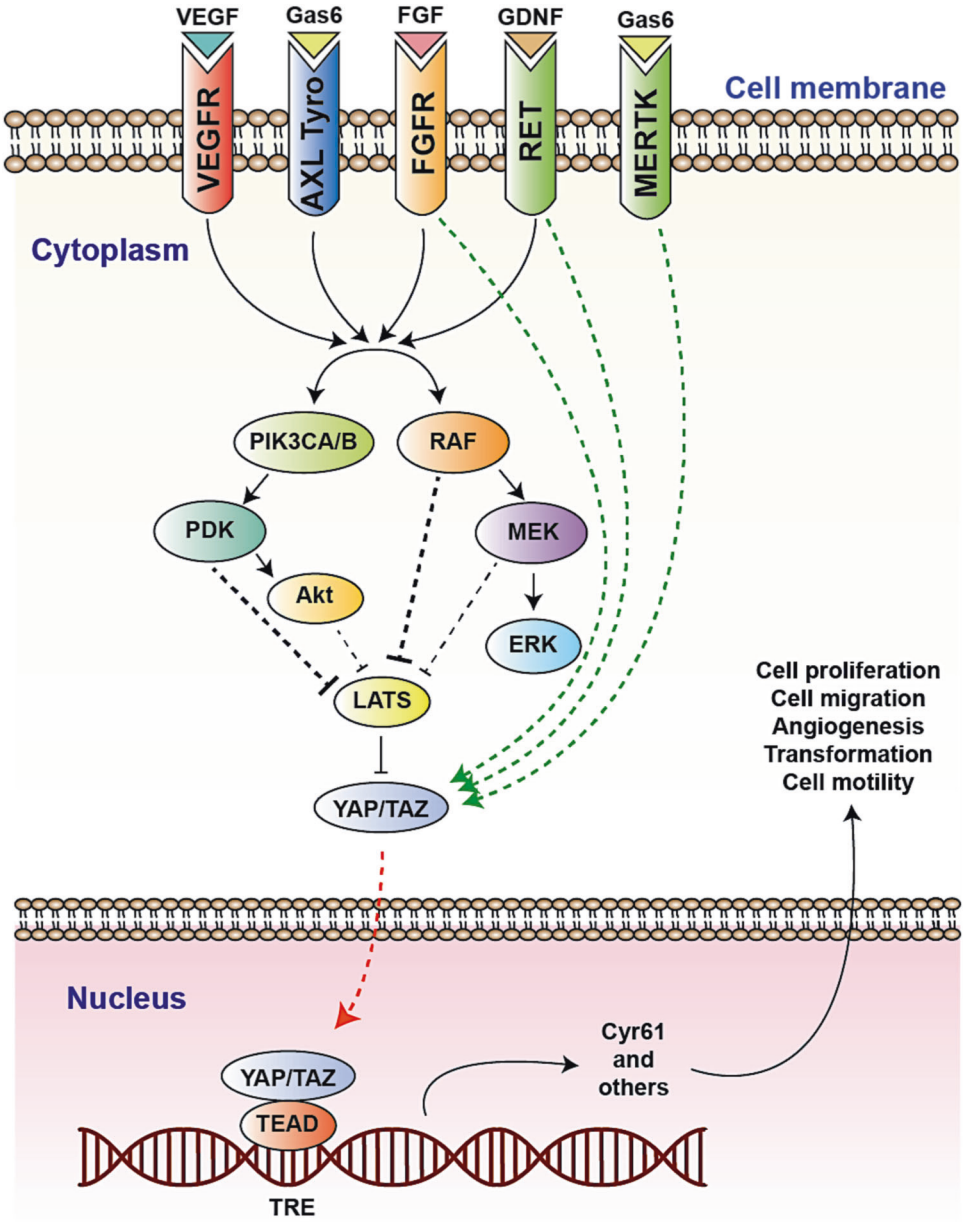

Fig. 8 Model of interaction between RTKs and the Hippo signaling pathway. RTKs regulate the Hippo pathway through PI3K and MAPK signaling pathways. Concurrently, some RTKs such as RET, MERTK, and FGFR, control YAP/TAZ function through direct interaction and tyrosine phosphorylation

downstream MAPK and PI3K signals (Fig. 8). Our findings have significant implications for our understanding of the crosstalk between RTKs and the Hippo pathway and their roles in cancer biology and therapy.

Methods

Plasmid construction and site-directed mutagenesis

RTK ORFs in pDONR-223 Gateway® entry vectors were transferred into destination expression plasmids using Gateway® Technology (Gateway™ LR Clonase™ Enzyme mix, ThermoFisher #11791100) to make the library. RTK plasmids were confirmed by double digestion and western blot analysis. Mutants were made using overlapping PCR. For lentivirus production, RET, FGFR1/2, AXL, TYRO3, MERTK, or VEGFR1/2 cDNA were cloned into pWPI lentiviral vector. To make GST-fusion proteins, oligos coding for different YAP fragments were cloned into the BamHI/NotI sites of pGEX-4T1. For making knockout cells single guided RNAs (sgRNAs) were cloned into Lenti-CRISPR v1. pBiT2.1-C (TK-SmBiT) and pBiT1.1-N (LgBiT) from Promega was used to make FGFR-YAP biosensor. Primers and oligos used for cloning are available in Supplementary Table 3.

Fusion protein production

BL21 bacterial cells were used to express pGEXT-4T1 constructs in 2xYT media. When the $OD_{600} < 1$, 0.4 mM IPTG (isopropyl β-D-1 thiogalactopyranoside) was added to induce fusion protein expression. Sixteen hours after induction at 20 °C, bacterial cells were harvested and lysed by sonication. Triton X-100 was added to the samples for a final concentration of 1% and samples were mixed on a rotator at 4 °C for 0.5–2 h. GST-fusion proteins were purified with glutathione–sepharose beads.

Cell culture

SH-SY5Y (human neuroblastoma), BHE (human lung adenocarcinoma), HeLa (human cervical adenocarcinoma), A549 (human lung adenocarcinoma), HEK293 (human embryonic kidney), HEK293A, and HEK293T cells were cultured in Dulbecco's modified Eagle's medium (DMEM; Sigma D6429) containing 10% FBS, and 1% P/S (Invitrogen). For MDA-MB231 and Hs578T (invasive ductal breast carcinoma) cells, DMEM was supplemented with 10% FBS, 1% P/S, and 1% nonessential amino acids (Sigma M7145). MCF10A (non-tumorigenic mammary epithelial cells) were maintained in DMEM/F12 medium (Sigma D6421) containing 5% horse serum (Sigma H1270), 0.25 mM L-glutamine (Sigma G7513), 10 µg/mL insulin (Sigma I6634), 20 ng/mL hEGF (Sigma E4269), 100 ng/mL cholera toxin (Sigma C8052), 0.5 µg/mL hydrocortisone (Sigma H4001), and 1% P/S. BOEC, and HUVEC (Lonza CC-2519 pooled donor) were cultured in cEGM-2 media (Lonza). HCT116 (colorectal carcinoma) cells were cultured in McCoy's 5a medium (Sigma M4892) supplemented with 10% FBS. All cells were grown at 37 °C with 5% CO_2. H1975 cells were cultured in RPMI-1640 Medium (Sigma R8758) containing 10% FBS and 1% P/S (Invitrogen).

RNA extraction and quantitative reverse transcriptase PCR (qRT-PCR)

Cells were grown in 35-mm or six-well plates to 70–90% confluency. RNA was purified using RNAzol RT reagent (Molecular Research Center, Inc., Cincinnati, OH, USA) (200 µL/well) according to the manufacturer's protocol. qRT-PCR was performed using the SuperScript III Platinum SYBR Green One-Step qRT- PCR Kit (Invitrogen) (50 ng RNA/reaction). 18S rRNA was used as an internal control. Primers used for qRT-PCR are available in Supplementary Table 4.

In vitro kinase assay

One hundred nanograms of recombinant truncated active forms of FGFR1, FGFR2, or RET kinase (SignalChem#F0413G, F0511G05, R02-11H-05) in kinase assay buffer (20 mM Tris-HCl pH 7.4, 10 mM MgCl2, 1 mM dithio- threitol, 1 mM EDTA, 100 µM sodium vanadate, 5 µM ATP) was incubated for 20 min at 30 °C with 0.5 µg of GST-fusion proteins. One fourth of the proteins were subjected to western blot analysis and the remainder was used for Ponceau S staining.

Protein extraction, antibodies, and western blotting

Methods for western blotting are as previously described [11]. Antibodies and corresponding dilutions are as follows: mouse monoclonal anti-TAZ (560235, BD Biosciences, 1:1000); rabbit polyclonal anti-YAP (sc-15407, Santa Cruz H125, 1:1000); mouse monoclonal anti-β-actin (A5441, Sigma, 1:10,000); rabbit monoclonal anti-phospho-TAZ Ser89 (E1X9C, cell signaling, 1:1000); rabbit monoclonal anti-cleaved PARP (ab32064, Abcam, 1:1000); rabbit polyclonal anti-CYR61 (sc-13100, Santa Cruz, 1:1000); rabbit monoclonal anti-luciferase (ab185923, Abcam, 1:1000); rabbit polyclonal anti-HA (H6908, Sigma, 1: 1000); mouse monoclonal anti-FLAG (F1804, Sigma, 1:1000); mouse monoclonal anti-Myc (9E10) (11667203001, Roche, 1:1000); rabbit polyclonal anti-phospho YAP (S127) (4911, Cell Signaling, 1:1000); rabbit monoclonal anti-LATS1 (3447, Cell Signaling, 1:1000); rabbit monoclonal anti-ERK1/2 (4695, Cell Signaling, 1:1000); mouse monoclonal anti-AKT (2967, Cell Signaling, 1:1000); rabbit monoclonal anti-phospho-AKT (Ser473) (4060, Cell Signaling, 1:1000); rabbit monoclonal anti-phospho-ERK (4370, Cell Signaling, 1:1000); rabbit monoclonal anti-phospho-MST1 (Ser183) (3681, Cell Signaling, 1:1,000); rabbit monoclonal anti-MST1 (3682, Cell Signaling, 1:1000); rabbit monoclonal anti-phospho-LATS1 (Thr1079) (8654, Cell Signaling, 1:1000); rabbit monoclonal anti-phospho-VEGFR2 (3770, Cell Signaling, 1:1000); rabbit monoclonal anti-VEGFR2 (2479, Cell Signaling, 1: 1000); mouse monoclonal anti-phosphotyrosine 4G10 (Millipore, 1: 1000); rabbit polyclonal anti-phospho-RET (Tyr905)(3221, Cell Signaling, 1:1000); rabbit monoclonal anti-RET (EIN8X, 14556 or D3D8R, 14698, Cell Signaling, 1:1000), and RET51-specific (EPR2871) rabbit monoclonal anti-RET51 (Abcam, ab134100, 1:1000) antibody; rabbit monoclonal anti-FGFR1 (D8E4, Cell Signaling, 1:1000); rabbit monoclonal anti-FGFR2 (D4H9, Cell Signaling, 1:1000); rabbit monoclonal anti-AXL (C89E7, Cell Signaling, 1:1000); rabbit monoclonal anti-phospho-AXL (D12B2, Cell Signaling, 1:1000); mouse monoclonal anti-TAZ (M2616, BD Bioscience, 1:1000); and mouse monoclonal anti-YAP (63.7, Santa Cruz, 1:1000).

Cell proliferation assay

A total of 2×10^3 cells were seeded in triplicate into each well of 12-well plates 24 h after transient transfection of

siRNAs or addback constructs or treatment with Dox (doxycycline, 1 μg/mL, BioShop, Canada). Cell numbers were counted on days 2, 4, and 6 after plating. Dox and/or ligand (200 ng/mL for FGF, VEGF, or Gas6) was refreshed every 2 days by changing with fresh culture media including 2% serum. Experiments were repeated at least three times. Data are shown as means ± S.D.

Soft agar assay

MDA-MB-231 cells (1×10^4 cells/well of six-well plate) were plated in 2% FBS-containing media with 0.4% agarose overtop of a 0.8% agarose layer. Medium was replaced every 3 days. Colonies were visible between 20–30 days. Colonies were stained with crystal violet (0.005% crystal violet in 20% methanol) and imaged under white light using the Bio-Rad Gel Doc System (Bio-Rad) and quantified using Quantity one software.

Clonogenic assay

A total of 2×10^5 BHE cells were seeded in a 12-well plate. Two hundred nanograms YAP-3YE/TAZ2YE or YAP-3YF/TAZ2YF siRNA-resistant constructs were transfected into siYAP/siTAZ knock down cells. The next day, 1000 cells were seeded in six-well plates. After 9 days, cells were fixed with 100% cold methanol for 5 min and stained with 0.05% Crystal violet in 25% methanol. Some samples were treated with 200 ng/mL FGF during the experiment.

Luciferase assay

One hundred nanograms of LATS-BS or STBS-Luc reporter was transfected alone or with each RTK from the RTK library into HEK293 cells in 12-well plates using Polyjet transfection reagent (SignaGen SL100688) according to the manufacturer's instructions. Five hundred nanograms was used for transfection of SmBiT-FGFR1/2 and/or LgBiT-YAP. After a 16 h incubation, media was removed and replaced with complete media. Forty-eight hours after transfection, the cells were lysed using passive lysis buffer and luciferase assays were performed using a Luciferase Assay Kit (Promega) and Turner Biosystems 20/20 luminometer. Luciferase fold-change was calculated based on the ratio of luciferase activity of the LATS-BS, STBS-Luc reporter, or YAP-FGFR biosensor to that of vector control. The data presented are the means of three independent experiments.

Lentivirus production, purification, and infection

A total of 1.5×10^7 HEK293T cells were seeded per 15 cm plate coated with poly-L-lysine (Sigma 7890) and incubated for 24 h. Cells were then transfected with 7.5 μg of transferring vector (pWPI or pTRIPZ), 6 μg of packaging plasmid (psPAX), and 2 μg of envelope plasmid (pMD2G) using Polyjet transfection reagent (Signagen SL100688) according to the manufacturer's instructions. The next day, media was removed and replaced with fresh media containing 10 nM NaButyrate. After 24 h incubation, the virus-containing media was collected, passed through a 0.45 μm filter, and concentrated using Lenti-X Concentrator (Clontech 631231). About 100 μL of 10× concentrated virus was used to infect 40–50% confluent cells in six-well plates in the presence of 8 μg/mL polybrene. Two days after infection, cells were selected with 1 μg/mL puromycin or 300 μg/mL hygromycin B.

Immunofluorescence

A total of $2–9 \times 10^4$ cells/mL were seeded into each well of a 24-well plate and grown to 70–80% confluency prior to transfection. Cells were serum-starved for at least 24 h before ligand/inhibitor treatment. Cells were treated with or without the following ligands and inhibitors: FGF (Sino Biological Inc. 10013-HNAE), VEGF (Sino Biological Inc. 10008-HNAE), Gas6 (R&D Systems, Recombinant Human Gas6 Protein, CF 885-GSB-050), GDNF (100 ng/mL, Peprotech, 450-10,Rocky Hill NJ), retinoic acid (RA) (5 μM, Sigma Aldrich, R2625), RET inhibitor (vandetanib, 10 μM, LC Laboratories, V9402), FGFR inhibitor (FIN-2, BGJ398, CH5183284), TAM inhibitor (LDC1267), MEK inhibitor (PD98059), AKT inhibitor (Triciribine), PDK inhibitor (GSK2334470), PI3K inhibitor (LY249002), RAF inhibitor (LY3009120), and VEGFR inhibitor (Axitinib). Some samples were treated with 10 uM inhibitor 3 h before and during ligand treatment. For staining, cells were fixed using 200 μL of 4% PFA and incubated at room temperature for 10 min. Cells were then permeabilized in 200 μL of 0.2% Triton X-100/PBS for 2 min. Primary and secondary antibodies were diluted in 1× PBS with 1% bovine serum albumin and 10% goat serum. The same conditions were used for aortic ring staining. The following antibodies were used: mouse monoclonal anti-YAP (Santa Cruz 101199, 1:300), mouse monoclonal anti-TAZ (BD Biosciences, 1:400), rabbit monoclonal anti-FGFR1 (D8E4, Cell Signaling, 1:100), mouse monoclonal anti-VE-cadherin (Santa Cruz F-8, 1:100), Alexa Fluor (AF)-555 rabbit anti-mouse IgG, and AF-488 goat anti-rabbit IgG. Images were captured using an inverted Nikon TE-2000U microscope (Melville, NY, USA).

siRNA/CRISPR-mediated gene knockdown/knockout

siRNA duplexes targeting YAP and TAZ, and an siRNA with scrambled sequence (siCtrl) were purchased from IDT.

The sequences of siYAP and siTAZ are as described [21]. All cells were transfected with 100 nM siRNAs using GenMute (Signagen, SL100568) according to the manufacturer's instructions. Two days after transfection, cells were collected for functional experiments. CRISPR-Cas9 constructs for TAZ knockout were generated using the lentiCRISPR v1 vector. Clonal cell lines were established by limiting dilution plating. Followings are oligo sequences for the cloning of sgRNA targeting TAZ (sgTAZ): sgTAZ-1-F: 5′-CACCGGAGGCTTACCGAGATTTGGC-3′; sgTAZ-1-R: 5′-AAACGCCAAATCTCGGTAAG CCTCC-3′; sgTAZ-2-F: 5′-CACCGTGCGCCAAGAGGAGCTCATG-3′; sgTAZ-2-R: 5′-AAACCAT GAGCTCCTCTTGGCGCAC-3′.

Cell motility assay

A total of 3×10^4 SH-SY5Y cells were seeded per well of a 24-well plate in DMEM supplemented with 1% FBS and 5 μM RA and allowed to adhere for 18 h. Cells were then washed twice with 1× PBS and treated with media supplemented with 1% FBS and 5 μM RA with or without GDNF (100 ng/mL). Images were captured every 20 min for 24 h using an Incucyte Zoom System equipped with a 10× objective lens (Essen Bioscience, Ann Arbor, MI). Images were exported and aligned as previously described [63]. Individual cells were tracked using ImageJ software (Freeware, NIH) with the MTrack2 plugin. DiPer software [64] was used to determine mean squared displacement over time for a minimum of 100 cells counted/condition.

Matrigel tube formation assay and aortic ring angiogenesis assay

Matrigel tube formation assay and aortic ring angiogenesis assay were performed as described [24]. For rescue experiments nucleofection technology by Lonza was used to transiently express constructs in HUVEC cells.

Wound-healing assay

A total of 1×10^5 cells were seeded per well of a 24-well plate (Ibidi #82406) and grown until confluent. Complete media was changed to media supplemented with 2% FBS in the presence or absence of VEGF (200 ng/mL) or FGF (200 ng/mL). A wound was generated by removing the insert and images were captured at various time points using a Nikon TE-2000U (Melville, NY, USA) inverted microscope.

Statistical analysis

For all graphs, data are presented as mean ± SD unless otherwise indicated in the figure legends. Statistical comparisons between groups were performed using a Student's
t test or analysis of variance.

Acknowledgements This work was supported by grants from Canadian Institute of Health Research (CIHR#119325, 148629), Canadian Breast Cancer Foundation to XY and CIHR (CIHR#142303) to LMM. TA is supported by the Vanier Canada Graduate Scholarship and Ontario International Graduate Scholarship. HJJvR was supported by a Queen Elizabeth II Graduate Scholarship in Science and Technology. SMM was supported by a Master's CIHR award. SMM, TM, PK, and TA are supported by studentships from the Terry Fox Research Institute Training Program in Transdisciplinary Cancer Research. We thank Dr David Lillicrap and Dr Paula James for providing the HUVEC, Telo-HEC, and BOEC cells; Dr Camargo for STBS-luc reporter plasmid; Mina Ghahremani for help in making figures; Dr Abdi Ghafari for Aortic ring angiogenesis assay; Elham Ghourbanpour and Dr Lillicrap for helping in Nucleofection transfection; Dr Guan for providing us with HEK293A-LATS knockout cells, and Carrie Wei for help in analyzing motility assay; and Dr Peter Greer for reading the manuscript.

Author contributions TA, LMM and XY designed the study and individual experiments. TA, KN, HJJvR, SMM, LW, YH, JY and PK performed experiments with supervision from XY and LMM. XY and LMM provided resources/equipment and secured funding. TA and XY wrote the manuscript.

Compliance with ethical standards

Conflict of interest The authors declare that they have no conflict of interest.

Publisher's note: Springer Nature remains neutral with regard to jurisdictional claims in published maps and institutional affiliations.

References

1. Moroishi T, Hansen CG, Guan K-L. The emerging roles of YAP and TAZ in cancer. Nat Rev Cancer. 2015;15:73.
2. Taha Z, J Janse van Rensburg H, Yang X. The Hippo Pathway: Immunity and Cancer. Cancers. 2018;10:94.
3. Johnson R, Halder G. The two faces of Hippo: targeting the Hippo pathway for regenerative medicine and cancer treatment. Nat Rev Drug Discov. 2014;13:63.
4. Azad T, Ghahremani M, Yang X. The role of YAP and TAZ in angiogenesis and vascular mimicry. Cells. 2019;8:407.
5. van Rensburg HJJ, Lai D, Azad T, Hao Y, Yang X. TAZ enhances mammary cell proliferation in 3D culture through transcriptional regulation of IRS1. Cell Signal. 2018;52:12–22.
6. Zhao Y, Montminy T, Azad T, Lightbody E, Hao Y, SenGupta S, et al. PI3K positively regulates YAP and TAZ in mammary tumorigenesis through multiple signaling pathways. Mol Cancer Res. 2018;16:1046–58.
7. Justice RW, Zilian O, Woods DF, Noll M, Bryant PJ. The *Drosophila* tumor suppressor gene warts encodes a homolog of human myotonic dystrophy kinase and is required for the control of cell shape and proliferation. Genes Dev. 1995;9:534–46.
8. Wu S, Huang J, Dong J, Pan D. Hippo encodes a Ste-20 family protein kinase that restricts cell proliferation and promotes apoptosis in conjunction with salvador and warts. Cell. 2003;114:445–56.

9. Tapon N, Harvey KF, Bell DW, Wahrer DC, Schiripo TA, Haber DA, et al. Salvador promotes both cell cycle exit and apoptosis in *Drosophila* and is mutated in human cancer cell lines. Cell. 2002;110:467–78.
10. Lai ZC, Wei X, Shimizu T, Ramos E, Rohrbaugh M, Nikolaidis N, et al. Control of cell proliferation and apoptosis by mob as tumor suppressor, mats. Cell. 2005;120:675–85.
11. Hao Y, Chun A, Cheung K, Rashidi B, Yang X. Tumor suppressor LATS1 is a negative regulator of oncogene YAP. J Biol Chem. 2008;283:5496–509.
12. Zhao B, Wei X, Li W, Udan RS, Yang Q, Kim J, et al. Inactivation of YAP oncoprotein by the Hippo pathway is involved in cell contact inhibition and tissue growth control. Genes Dev. 2007;21:2747–61.
13. Zhang X, Milton CC, Humbert PO, Harvey KF. Transcriptional output of the Salvador/warts/hippo pathway is controlled in distinct fashions in *Drosophila* melanogaster and mammalian cell lines. Cancer Res. 2009;69:6033–41.
14. Liu AM, Wong KF, Jiang X, Qiao Y, Luk JM. Regulators of mammalian Hippo pathway in cancer. Biochim et Biophys Acta. 2012;1826:357–64.
15. Saucedo LJ, Edgar BA. Filling out the Hippo pathway. Nat Rev Mol Cell Biol. 2007;8:613–21.
16. Chen L, Chan SW, Zhang X, Walsh M, Lim CJ, Hong W, et al. Structural basis of YAP recognition by TEAD4 in the hippo pathway. Genes Dev. 2010;24:290–300.
17. Gumbiner BM, Kim NG. The Hippo-YAP signaling pathway and contact inhibition of growth. J Cell Sci. 2014;127:709–17.
18. Reddy B, Irvine KD. Regulation of Hippo signaling by EGFR-MAPK signaling through Ajuba family proteins. Dev Cell. 2013;24:459–71.
19. Schlessinger J. Receptor tyrosine kinases: legacy of the first two decades. Cold Spring Harb Perspect Biol. 2014;6:89–112.
20. Choura M, Rebaï A. Receptor tyrosine kinases: from biology to pathology. J Recept Signal Transduct. 2011;31:387–94.
21. Arteaga CL, Engelman JA. ERBB receptors: from oncogene discovery to basic science to mechanism-based cancer therapeutics. Cancer Cell. 2014;25:282–303.
22. Ullrich A, Schlessinger J. Signal transduction by receptors with tyrosine kinase activity. Cell. 1990;61:203–12.
23. Robinson DR, Wu Y-M, Lin S-F. The protein tyrosine kinase family of the human genome. Oncogene. 2000;19:48–55.
24. Azad T, van Rensburg HJ, Lightbody ED, Neveu B, Champagne A, Ghaffari, et al. A LATS biosensor screen identifies VEGFR as a regulator of the Hippo pathway in angiogenesis. Nat Commun. 2018;9:10–61.
25. Azad T, Nouri K, van Rensburg Janse HJ, Hao Y, Yang X. Monitoring Hippo signaling pathway activity using a luciferase-based large tumor suppressor (LATS) biosensor. J Vis Exp. 2018;139:11–34.
26. Yang X, Boehm JS, Yang X, Salehi-Ashtiani K, Hao T, Shen Y, et al. A public genome-scale lentiviral expression library of human ORFs. Nat Methods. 2011;8:659–61.
27. Wang W, Li X, Huang J, Feng L, Dolinta KG, Chen J. Defining the protein–protein interaction network of the human Hippo pathway. Mol Cell Proteom. 2014;13:119–31.
28. Mohseni M, Sun J, Lau A, Curtis S, Goldsmith J, Fox VL, et al. A genetic screen identifies an LKB1-MARK signalling axis controlling the Hippo-YAP pathway. Nat Cell Biol. 2014;16:108–17.
29. Vasudevan HN, Soriano P. Curr Top Dev Biol. 2016;117:393–404.
30. Axelrod H, Pienta KJ. Axl as a mediator of cellular growth and survival. Oncotarget. 2014;5:8818–52.
31. Koorstra JBM, Karikari C, Feldmann G, Bisht S, Leal-Rojas P, Offerhaus GJA, et al. The Axl receptor tyrosine kinase confers an adverse prognostic influence in pancreatic cancer and represents a new therapeutic target. Cancer Biol Ther. 2009;8:618–26.
32. Hector A, Montgomery EA, Karikari C, Canto MI, Dunbar KB, Wang JS, et al. The Axl receptor tyrosine kinase is an adverse prognostic factor and a therapeutic target in esophageal adenocarcinoma. Cancer Biol Ther. 2010;10:1009–18.
33. Mulligan LM. RET revisited: expanding the oncogenic portfolio. Nat Rev Cancer. 2014;14:173–86.
34. Gainor JF, Shaw AT. Novel targets in non-small cell lung cancer: ROS1 and RET fusionsO. Oncologist. 2013;2:13–35.
35. Huang SM, Chen TS, Chiu CM, Chang LK, Liao KF, Tan HM, et al. GDNF increases cell motility in human colon cancer through VEGF–VEGFR1 interaction. Endocr Relat Cancer. 2014;21:73–84.
36. Romei C, Ciampi R, Elisei R. A comprehensive overview of the role of the RET proto-oncogene in thyroid carcinoma. Nat Rev Endocrinol. 2016;12:192–202.
37. Ishida M, Ichihara M, Mii S, Jijiwa M, Asai N, Enomoto A, et al. Sprouty2 regulates growth and differentiation of human neuroblastoma cells through RET tyrosine kinase. Cancer Sci. 2007;98:815–21.
38. Hofstra RM, Landsvater RM, Ceccherini I, Stulp RP, Stelwagen T, Luo Y, et al. A mutation in the RET proto-oncogene associated with multiple endocrine neoplasia type 2B and sporadic medullary thyroid carcinoma. Nature. 1994;367:375–414.
39. Cavallaro U, Christofori G. Cell adhesion and signalling by cadherins and Ig-CAMs in cancer. Nat Rev Cancer. 2004;4:118–35.
40. Carmeliet P, Jain RK. Molecular mechanisms and clinical applications of angiogenesis. Nature. 2011;473:298–320.
41. Lemmon MA, Schlessinger J. Cell signaling by receptor tyrosine kinases. Cell. 2010;141:1117–34.
42. Fan R, Kim N-G, Gumbiner BM. Regulation of Hippo pathway by mitogenic growth factors via phosphoinositide 3-kinase and phosphoinositide-dependent kinase-1. Proc Natl Acad Sci USA. 2013;110:2569–74.
43. Romano D, Nguyen LK, Matallanas D, Halasz M, Doherty C, Kholodenko, et al. Protein interaction switches coordinate Raf-1 and MST2/Hippo signalling. Nat Cell Biol. 2014;16:673–701.
44. Calses PC, Crawford JJ, Lill JR, Dey A. Hippo pathway in cancer: aberrant regulation and therapeutic opportunities. Trends Cancer. 2019;5:297–307.
45. Haskins JW, Nguyen DX, Stern DF. Neuregulin 1–activated ERBB4 interacts with YAP to induce Hippo pathway target genes and promote cell migration. Sci Signal. 2014;7:116–26.
46. Keshet R, Reuven N, Shaul Y. c-Abl forces YAP to switch sides. Mol Cell Oncol. 2015;2:99–106.
47. Sugihara T, Werneburg NW, Hernandez MC, Yang L, Kabashima A, Hirsova P, et al. YAP tyrosine phosphorylation and nuclear localization in cholangiocarcinoma cells is regulated by LCK and independent of LATS activity. Mol Cancer Res. 2018;2:158–72.
48. Li, P, Silvis, MR, Honaker, Y, Lien, WH, Arron, ST, Vasioukhin, V. αE-catenin inhibits a Src–YAP1 oncogenic module that couples tyrosine kinases and the effector of Hippo signaling pathway. Genes Dev. 2016;30:798–811.
49. Levy D, Adamovich Y, Reuven N, Shaul Y. Yap1 phosphorylation by c-Abl is a critical step in selective activation of proapoptotic genes in response to DNA damage. Mol Cell. 2008;29:350–61.
50. Yu F-X, Guan K-L. The Hippo pathway: regulators and regulations. Genes Dev. 2013;27:355–71.
51. Attisano L, Wrana JL. Signal integration in TGF-β, WNT, and Hippo pathways. F1000Prime Rep. 2013;5:17–26.
52. Yu FX, Zhao B, Panupinthu N, Jewell JL, Lian I, Wang LH, et al. Regulation of the Hippo-YAP pathway by G-protein-coupled receptor signaling. Cell. 2012;150:780–91.

53. Rizvi S, Yamada D, Hirsova P, Bronk SF, Werneburg NW, Krishnan A, et al. A hippo and fibroblast growth factor receptor autocrine pathway in cholangiocarcinoma. J Biol Chem. 2016;115:72–98.
54. Edwards DN, Ngwa VM, Wang S, Shiuan E, Brantley-Sieders DM, Kim LC, et al. The receptor tyrosine kinase EphA2 promotes glutamine metabolism in tumors by activating the transcriptional coactivators YAP and TAZ. Sci Signal. 2017;10:46–67.
55. Meng Z, Moroishi T, Mottier-Pavie V, Plouffe SW, Hansen CG, Hong AW, et al. MAP4K family kinases act in parallel to MST1/2 to activate LATS1/2 in the Hippo pathway. Nat Commun. 2015;6:57–83.
56. Moroishi T, Park HW, Qin B, Chen Q, Meng Z, Plouffe SW, et al. A YAP/TAZ-induced feedback mechanism regulates Hippo pathway homeostasis. Genes Dev. 2015;29:1271–84.
57. Xu MZ, Chan SW, Liu AM, Wong KF, Fan ST, Chen J, et al. AXL receptor kinase is a mediator of YAP-dependent oncogenic functions in hepatocellular carcinoma. Oncogene. 2011;30:1229.
58. Tamm C, Böwer N, Annerén C. Regulation of mouse embryonic stem cell self-renewal by a Yes− YAP− TEAD2 signaling pathway downstream of LIF. J Cell Sci. 2011;124:1136–44.
59. Jang EJ, Jeong H, Han KH, Kwon HM, Hong JH, Hwang ES, et al. TAZ suppresses NFAT5 activity through tyrosine phosphorylation. Mol Cell Biol. 2012;32:4925–32.
60. Chioni A-M, Grose R. FGFR1 cleavage and nuclear translocation regulates breast cancer cell behavior. J Cell Biol. 2012;197:801–17.
61. Lee YW, Terranova C, Birkaya B, Narla S, Kehoe D, Parikh A, et al. A novel nuclear FGF receptor-1 partnership with retinoid and Nur receptors during developmental gene programming of embryonic stem cells. J Cell Biochem. 2012;113:2920–36.
62. Coleman SJ, Chioni AM, Ghallab M, Anderson RK, Lemoine NR, Kocher HM, et al. Nuclear translocation of FGFR1 and FGF2 in pancreatic stellate cells facilitates pancreatic cancer cell invasion. EMBO Mol Med. 2014;6:467–81.
63. Lian EY, Maritan SM, Cockburn JG, Kasaian K, Crupi MJ, Hurlbut D, et al. Differential roles of RET isoforms in medullary and papillary thyroid carcinomas. Endocr Relat Cancer. 2017;24:53–69.
64. Gorelik R, Gautreau A. Quantitative and unbiased analysis of directional persistence in cell migration. Nat Protoc. 2014;9:1931–43.